iScience

CellPress
OPEN ACCESS

Article

Translational Components Contribute to Acclimation Responses to High Light, Heat, and Cold in *Arabidopsis*

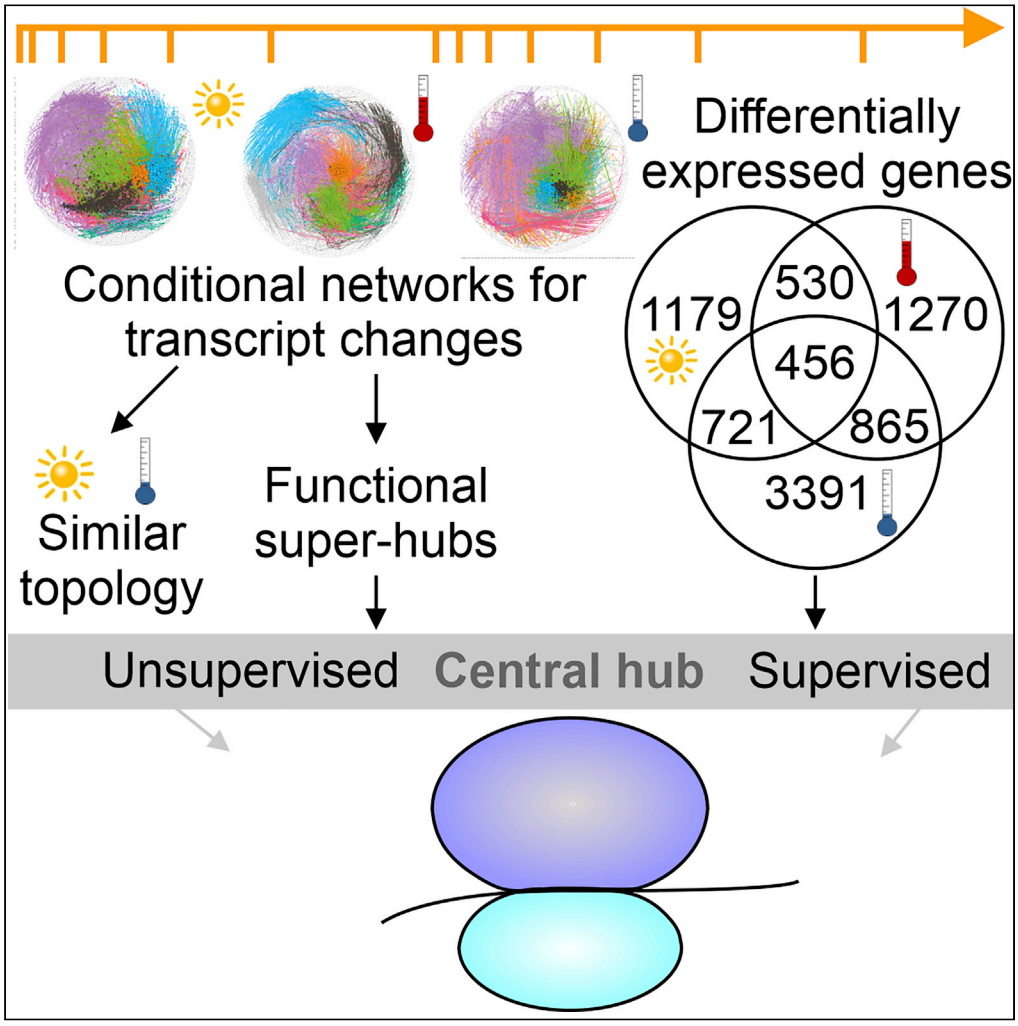

Antoni Garcia-Molina, Tatjana Kleine, Kevin Schneider, Timo Mühlhaus, Martin Lehmann, Dario Leister

leister@lmu.de

HIGHLIGHTS

Time series of acclimation and de-acclimation without pleiotropic stresses

Kinetics of transcriptomes and metabolomes under three environmental conditions

Transcriptomes return to a baseline, but HL and heat metabolomes do not

All acclimation responses involve the translational machinery and photosynthesis

Garcia-Molina et al., iScience *23*, 101331
July 24, 2020
https://doi.org/10.1016/j.isci.2020.101331

iScience

CellPress
OPEN ACCESS

Article

Translational Components Contribute to Acclimation Responses to High Light, Heat, and Cold in *Arabidopsis*

Antoni Garcia-Molina,[1,3] Tatjana Kleine,[1,3] Kevin Schneider,[2] Timo Mühlhaus,[2] Martin Lehmann,[1] and Dario Leister[1,4,*]

SUMMARY

Plant metabolism is broadly reprogrammed during acclimation to abiotic changes. Most previous studies have focused on transitions from standard to single stressful conditions. Here, we systematically analyze acclimation processes to levels of light, heat, and cold stress that subtly alter physiological parameters and assess their reversibility during de-acclimation. Metabolome and transcriptome changes were monitored at 11 different time points. Unlike transcriptome changes, most alterations in metabolite levels did not readily return to baseline values, except in the case of cold acclimation. Similar regulatory networks operate during (de-)acclimation to high light and cold, whereas heat and high-light responses exhibit similar dynamics, as determined by surprisal and conditional network analyses. In all acclimation models tested here, super-hubs in conditional transcriptome networks are enriched for components involved in translation, particularly ribosomes. Hence, we suggest that the ribosome serves as a common central hub for the control of three different (de-)acclimation responses.

INTRODUCTION

Plants continuously adapt to abiotic environmental changes by acclimation, but even moderate deviations from the optimum can markedly limit crop yields (Ashraf et al., 2012; Buchanan et al., 2000; Lobell and Gourdji, 2012; Reddy, 2015). In the era of global warming, acclimation becomes even more relevant, as plants encounter progressive environmental changes (Anjum, 2015). Therefore, a comprehensive understanding of plant acclimation responses is required to design strategies that stabilize or enhance yields in increasingly hostile environments.

Acclimation can act on timescales that vary from minutes to days; involves the modification of gene expression, protein activity, and metabolite profiles; and ultimately affects all cellular compartments (Beine-Golovchuk et al., 2018; Caldana et al., 2011; Kaplan et al., 2007; Mueller et al., 2015; Suzuki et al., 2015; Vogel et al., 2014; Zandalinas et al., 2019; Zhao et al., 2017). Acclimation-associated physiological changes can be divided into three phases. In the first phase, environmental changes immediately affect cellular reactions (Karpinski et al., 2013; Mullineaux and Karpinski, 2002; Schmitz et al., 2014), perturbing metabolism by inhibition/activation of metabolic reactions, and leading to dearth/excess of substrates or products, increased demand for specific compounds, or a combination of these factors. Well-known examples are the acidification of the chloroplast lumen during exposure to high light (HL) levels, which activates photoprotective mechanisms such as non-photochemical quenching (NPQ) (Pinnola and Bassi, 2018; Ruban, 2016), and protein misfolding induced by heat (Guy et al., 1997; Park and Seo, 2015; Wang et al., 2004). Transient changes occur during the second phase, reconfiguring primary and energy metabolism by accumulating protective compounds and balancing levels of reactive oxygen species (Foyer et al., 2009; Nishizawa et al., 2008; Noctor et al., 2011; Panikulangara et al., 2004). Carbohydrates are re-allocated to sustain metabolic demands (Dyson et al., 2015; Nägele and Heyer, 2013; Patzke et al., 2019) and secondary metabolism is also redirected, to produce anthocyanins in response to HL or cold, for instance (Grotewold, 2006; Schulz et al., 2016; Speiser et al., 2015). Under prolonged environmental change, a new steady state is eventually established (third phase) (Huang et al., 2019; Kaplan et al., 2004; Wang et al., 2020).

[1]Plant Molecular Biology, Faculty of Biology, Ludwig-Maximilians-University Munich, Großhadernerstraße 2-4, 82152 Planegg-Martinsried, Germany

[2]Computational Systems Biology, TU Kaiserslautern, Paul-Ehrlich-Straße 23, 67663 Kaiserslautern, Germany

[3]These authors contributed equally

[4]Lead Contact

*Correspondence: leister@lmu.de

https://doi.org/10.1016/j.isci.2020.101331

Owing to the complexity of the process, enhancing acclimation by altering the activity of single components can have unexpected consequences. For instance, overexpressing the same three photoprotective proteins in two different species has opposite effects on growth under natural conditions (Garcia-Molina and Leister, 2020; Kromdijk et al., 2016), most likely due to interspecific differences in acclimation and metabolic networks. Therefore, system-wide approaches are needed to dissect acclimation responses, so as to ensure that targeted modifications occur with minimal trade-offs. Various studies of transcriptomic, proteomic, and metabolomic responses to changes in light or temperature have been done in *Arabidopsis thaliana* (hereafter *Arabidopsis*) (Caldana et al., 2011; Carrera et al., 2017; Hannah et al., 2005; Higashi et al., 2015; Huang et al., 2019; Kaplan et al., 2004, 2007; Larkindale and Vierling, 2008; Rossel et al., 2002; Wang et al., 2020), but few of them considered more than one environmental condition (Caldana et al., 2011; Carrera et al., 2017; Cerny et al., 2014; Kaplan et al., 2004; Rocco et al., 2013) or the return from stressful to control conditions (de-acclimation) (Kaplan et al., 2004; Miki et al., 2018; Nakaminami et al., 2014; Pagter et al., 2017; Vyse et al., 2019; Zuther et al., 2015, 2019).

To fill this gap, we have comprehensively monitored physiological, metabolomic, and transcriptomic changes in plants during acclimation and subsequent de-acclimation to HL, heat, and cold. Our study reveals that altered metabolic steady states are established during acclimation, which persist after de-acclimation, whereas transcriptome changes are partially (HL and heat) or fully (cold) reversible. Bioinformatic analyses indicate that components of translation, especially ribosomal proteins (RPs), play central roles in acclimation to changes in the abiotic environment.

RESULTS

Design of Acclimation and De-acclimation Kinetics

To study how the model plant *Arabidopsis* acclimates to omnipresent changes in temperature and light intensity, we looked at the effects of increased light level (HL) and suboptimal temperature (heat or cold). As the standard growth condition ("control condition"), we used a long photoperiod (16 h/8 h day/night) with temperatures of 18°C at night and 22°C during the day. Plants were grown under light-emitting diode (LED) lights to avoid unwanted heat development and ensure reproducibility among independent replicates (LEDs have a longer half-life than fluorescent tubes). Plant growth and development were optimal at light intensities of 80 μmol photons m^{-2} s^{-1} (Figures S1A–S1C), and this level was used as our control condition.

Young *Arabidopsis* plants are reported to display 50% photoinhibition at a photosynthetically active radiation (PAR) of 535 μmol photons m^{-2} s^{-1} (Carvalho et al., 2015) and possess a basal thermotolerance ranging from −4°C to 44°C (Kaplan et al., 2004). To establish moderate acclimation conditions that do not irreversibly affect plant development, we first tested different light intensities. To this end, 14-day-old plants grown under control conditions were subjected to a PAR level of 450 or 800 μmol photons m^{-2} s^{-1} for 7 days and their physiological responses were recorded. Intensities of 450 μmol photons m^{-2} s^{-1} had a minimal impact on plant growth, whereas those of 800 μmol photons m^{-2} s^{-1} limited growth and led to anthocyanin accumulation within 4 days (Figure S1B). To evaluate photoinhibition, we monitored the maximum quantum yield of photosystem II (PSII) (Fv/Fm) during the 4 days of HL treatment, followed by 4 more days under control conditions to assess reversibility. Compared with control conditions (Fv/Fm = 0.8 during the whole time course), plants exposed to 450 μmol photons m^{-2} s^{-1} exhibited photoinhibition, which reached its maximum after 3 days (Fv/Fm = 0.57), but was fully reversible during de-acclimation (Figure S1C and Table S1). At 800 μmol photons m^{-2} s^{-1}, photoinhibition was exacerbated (Fv/Fm = 0.58 after 1 day) and was only partially reversible (Figure S1C and Table S1). Therefore, 450 μmol photons m^{-2} s^{-1} was selected for the HL condition. Growth at 32°C throughout the light and dark phase resulted in the typically elongated petioles (Crawford et al., 2012; Sanchez-Bermejo et al., 2015) (Figure S1D) and control-like Fv/Fm values (Figure S1C) and served as the heat stress condition. Cold stress was imposed by reducing the growth temperature to 4°C, and decreasing the light intensity (35 μmol photons m^{-2} s^{-1}), as reported previously (Fowler and Thomashow, 2002; Hoermiller et al., 2017; Juszczak et al., 2016; Zuther et al., 2019), to avoid photoinhibition (Fv/Fm of 0.67 versus 0.79 after 4 days under 80 and 35 μmol photons m^{-2} s^{-1}, respectively; Figure S1C).

As 2-week-old plants grown under standard conditions returned to normal growth and development after 4 days each of acclimation and de-acclimation (Figure S1D), this design was used to systematically study reversible acclimation to HL, heat, and cold.

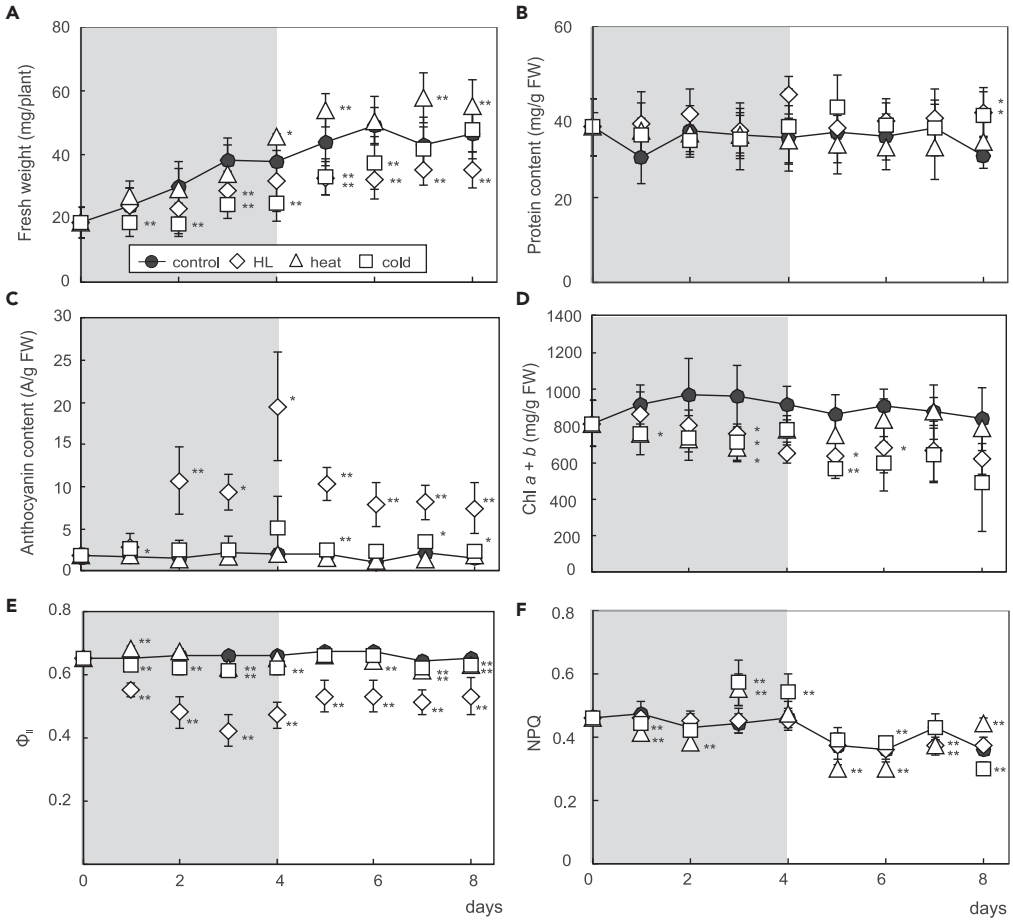

Figure 1. Physiological Performance of *Arabidopsis* Plants during (De-)acclimation to High Light, Heat, and Cold

(A–F) 14-day-old plants grown under standard growth conditions were exposed to high light (HL), heat, and cold for 4 days (acclimation period, highlighted by gray background), followed by a return to standard growth conditions for 4 days (de-acclimation period). Fresh weight (A), total protein content (B), anthocyanin content (C), chlorophyll (Chl *a* + *b*) level (D), effective quantum yield of photosystem II (Φ_{II}) (E), and non-photochemical quenching (NPQ) (F) were recorded daily. Values correspond to the mean ± SD of n ≥ 4 independent experiments. **p < 0.01; *p < 0.05 (Student's t test). See Table S1 for standard deviations and statistics. See also Figure S1.

Physiological Changes during (De-)acclimation

To monitor the effects of (de-)acclimation on plant development and physiology, we measured fresh weight (FW) and total proteins, anthocyanins, and chlorophylls (Figure 1 and Table S1). In all cases, FW of plants increased over the time course, e.g., from ~19 to ~47 mg/plant under standard conditions. In HL-exposed plants, the increase set in only on day 3 of the acclimation phase, but growth was partially restored during de-acclimation. Thus, heat-treated plants gained significantly more FW than control plants under standard conditions from day 4 of acclimation onward. Cold treatment affected FW increase most strongly, but the deficit relative to controls disappeared after 3 days of de-acclimation (Figure 1A and Table S1). HL- and cold-treated plants accumulated significantly increased levels of total proteins and anthocyanins; otherwise, these parameters were unchanged (Figures 1B and 1C). Conversely, average chlorophyll levels in treated plants were lower than in controls (Figure 1D). Photosynthetic performance was assessed in terms of the effective quantum yield of PSII (Φ_{II}) and NPQ. In general, Φ_{II} remained steady over the time course (0.62–0.67 depending on the treatment and time point), except for a progressive and significant decrease of Φ_{II} to 0.42 by day 3 of acclimation to HL, which was reversed almost completely during de-acclimation (0.53 on day 4) (Figure 1E and Table S1) and is seen in the behavior of Fv/Fm (Figure S1). This reflects the course of, and recovery from, photoinhibition (Yamori, 2016). Heat and cold each had significant effects on NPQ, in accordance with previous studies that used moderate levels of temperature stress (Harvaux and Kloppstech, 2001; Zhang et al., 2010) (Figure 1F).

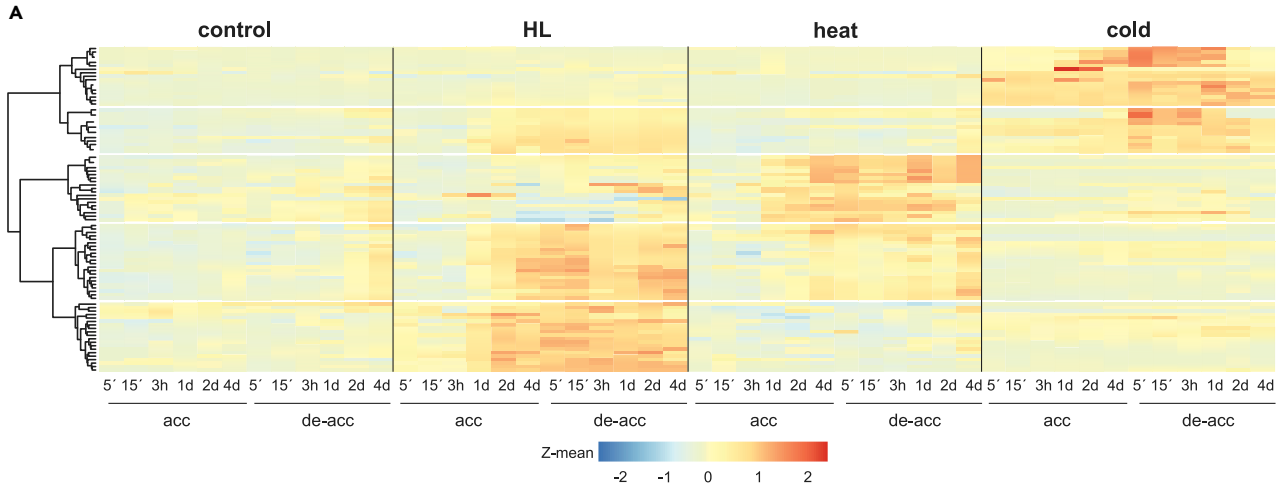
A
control
HL
heat
cold
5′ 15′ 3h 1d 2d 4d
acc
de-acc
Z-mean
-2 -1 0 1 2

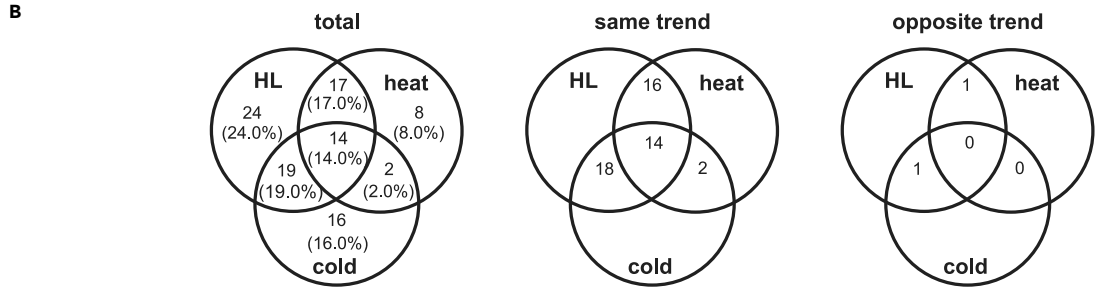
B
total
same trend
opposite trend
HL
heat
cold
24 (24.0%)
17 (17.0%)
8 (8.0%)
14 (14.0%)
19 (19.0%)
2 (2.0%)
16 (16.0%)
16
14
18
2
1
0
0

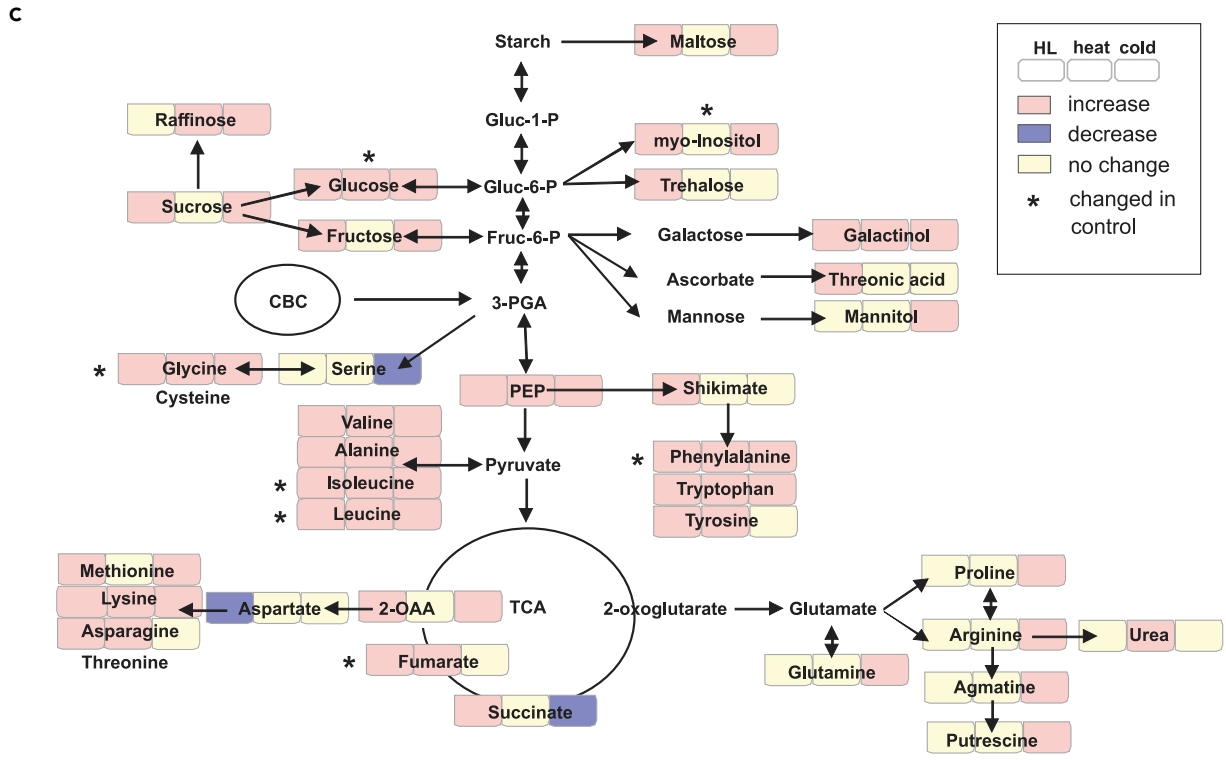
C
Starch
Maltose
Gluc-1-P
Raffinose
myo-Inositol
Glucose
Gluc-6-P
Trehalose
Sucrose
Fructose
Fruc-6-P
Galactose
Galactinol
Ascorbate
Threonic acid
CBC
3-PGA
Mannose
Mannitol
Glycine
Serine
Cysteine
PEP
Shikimate
Valine
Alanine
Isoleucine
Leucine
Pyruvate
Phenylalanine
Tryptophan
Tyrosine
Methionine
Lysine
Asparagine
Threonine
Aspartate
2-OAA
TCA
Fumarate
Succinate
2-oxoglutarate
Glutamate
Glutamine
Proline
Arginine
Urea
Agmatine
Putrescine
HL heat cold
increase
decrease
no change
changed in control

Figure 2. Changes in Metabolite Composition during (De-)acclimation to High Light, Heat, and Cold

(A) Heatmaps based on Z-means of fold changes of SAMs and generated by hierarchical clustering according to Ward d2.

(B) Venn diagrams depicting shared or unique SAMs, comprising total numbers (left panel, "total"), or only the ones that show the same (up-up or down-down, "same trend") or opposite (up-down or down-up, "opposite trend") regulation polarities.

(C) Scheme summarizing the changes in concentration of metabolites involved in central metabolism in *Arabidopsis*. acc, acclimation; de-acc, de-acclimation; CBC, Calvin-Benson cycle; TCA, tricarboxylic acid cycle; Gluc, glucose; Fruc, fructose; P, phosphate; 3-PGA, 3-phosphoglycerate; PEP, phosphoenolpyruvate; 2-OAA, 2-oxaloacetate. Metabolites whose levels also changed under control conditions are indicated by *. Note that glycine levels decreased under control conditions.

See also Figures S2 and S3.

Thus, in agreement with the restoration of growth after de-acclimation (see Figure S1), most physiological parameters monitored are reversed during de-acclimation experiments.

Molecular Changes during (De-)acclimation: Metabolite Profiling

To obtain a comprehensive picture of molecular changes at the metabolite level, plant material was harvested from shoots at several time points during (de-)acclimation (Figure S2). Because alterations in metabolite or transcript levels can occur rapidly upon exposure to sudden changes in environmental parameters (Caldana et al., 2011; Kaplan et al., 2007; Mueller et al., 2015; Suzuki et al., 2015; Vogel et al., 2014; Zandalinas et al., 2019), measurements were made at both early (1, 5, and 15 min and 3 h) and later time points (2 and 4 days). Samples from control plants grown in parallel and harvested at the same time points were always included.

Changes in metabolite levels were identified by gas chromatography (GC)-time-of-flight mass spectrometry (MS), and a total of 98 primary metabolites and 36 unidentified compounds were detected. "Significantly altered metabolites (SAMs)" were defined as metabolites that showed at least a 2-fold change (FC $\geq$ 2) in concentration relative to the value at time point 0 (Student's t test with a false discovery rate [FDR] $\leq$ 0.05). Under control conditions, 11 metabolites changed significantly; e.g., leucine, isoleucine, fumarate, and glucose increased, as expected, as plants got older (Chia et al., 2000). Under the acclimation treatments, numbers of SAMs began to increase within 1 or 2 days, and 74, 41, and 51 SAMs were noted for HL, heat, and cold conditions, respectively (Table S2 and Figure S3A).

To infer the dynamics of metabolome changes under each treatment, hierarchical clustering was used to generate heatmaps for all metabolites that changed significantly in level at least once in any (de-)acclimation experiment (Figure 2A). The heatmaps reflected the negligible changes in metabolites under control conditions, which only become discernible toward the end of the time course (Figure 2A). Following HL or heat treatment, 70%–80% of metabolome perturbations persisted during de-acclimation, but 90% returned to the initial state after cold exposure (Figures 2A and S3B and Table S2).

Venn diagrams revealed that the fraction of metabolites altered under two different treatments was similar or significantly higher (super exact test, Wang et al., 2015, $p = 0.03$) than that of metabolites that were exclusively altered by one treatment (Figure 2B). In all, 31 metabolites reacted to both HL and heat and 33 to both HL and cold, whereas 24, 8, and 16 metabolites were specifically altered under HL, heat, and cold, respectively. Furthermore, the vast majority of the first set responded in the same direction (increase or decrease), indicating that metabolome responses during acclimation to the different stress conditions can target overlapping sets of compounds.

In addition, levels of 14 metabolites were increased under all three conditions. Nine of these compounds are shown in an annotated integrative map of central metabolism in *Arabidopsis* (Figure 2C) and four of them are unknown. Taking into account the changed levels of some of these metabolites under control conditions (Table S2), galactinol, 3-phosphoglycerate (PEP) and the amino acids glycine, tryptophan, valine, alanine, and lysine are the metabolites whose levels are increased under all treatments (Figure 2C).

Sugars like glucose, sucrose, fructose, and maltose increased during HL and cold, and trehalose increased only during HL. Central organic acids, especially fumarate, which is one of the main carbon (C) storage compounds in *Arabidopsis* (Chia et al., 2000), and succinate, increased during exposure to HL, and 2-oxalacetate, during HL and cold (Figure 2C and Table S2). Thus the accumulation of C blocks that can store energy or provide skeletons for larger biomolecules is characteristic for the metabolic response to HL. Notably, fumarate was reported to be important for cold acclimation of 8-week-old plants grown under short-day

conditions and a light intensity of 100 μmol photons m^{-1} s^{-2} (Dyson et al., 2016). The only moderate increase of fumarate under our cold conditions could be attributable to the usage of young (2- to 3-week-old) plants exposed to long-day conditions and a lower light intensity of 35 μmol photons m^{-2} s^{-1}. In addition, the accumulation of compatible solutes like galactinol under all tested conditions, *myo*-inositol under HL and cold, raffinose under heat and cold, and mannitol and proline under cold points to a need to mitigate osmotic stress (Nishizawa et al., 2008; Panikulangara et al., 2004) (Figure 2C).

Overall, acclimation resulted in a general increase in amino acid pools under all treatments, and accumulation of carbohydrates and organic acids particularly under HL and cold treatment. Thus the relatively subtle alterations of physiological parameters (see Figure 1) are accompanied by marked and mostly irreversible (except in the case of cold stress) changes in metabolite levels.

Molecular Changes during (De-)acclimation: Transcript Profiling

Because only a subset of metabolites in a plant cell can be detected by GC-MS, we also performed transcript profiling, using RNA sequencing to track both nuclear and organellar transcripts. First, we studied the accumulation of *bona fide* marker mRNAs for the circadian clock and the cell cycle. Clearly, the circadian oscillations observed under control conditions were disrupted by the HL, heat, and cold treatments (Figure S4A), and the expression pattern of cell-cycle markers was altered (Figure S4B). In light of this, we refrained from direct treatment versus control comparisons between individual time points. Instead, transcripts were defined as originating from "differentially expressed genes (DEGs)" if they displayed an absolute FC $\geq$ 2 with an FDR $\leq$0.05 (Student's t test) compared with the t = 0 min time point. We identified 1,568 DEGs under control conditions, 4,731 under HL, 4,801 under heat, and 6,426 under cold conditions (Table S3 and Figure S5A). Transcriptome changes under standard conditions were attributed to circadian oscillations (365 and 648 DEGs after 3 h acclimation and de-acclimation) and advancing plant development at the last time point of the kinetics experiment (1,053 DEGs on day 4 of de-acclimation) (Figure S5A). Notably, HL had less effect on transcripts for heat shock proteins and heat shock factors than did heat or cold treatment (Figure S5B), indicating that our HL conditions did not impose heat stress on plants (Huang et al., 2019).

The general behavior of the transcriptomes during acclimation and de-acclimation phases was visualized in heatmaps, which showed limited transcriptome changes under control conditions, whereas marked changes in mRNA expression patterns appeared after 3 h and 2 days of acclimation (Figure 3A). Large gene sets (regulons) continued to be differentially expressed during de-acclimation, although in many instances the trend of regulation was reversed (Figure 3A). Indeed, the largest numbers of DEGs were observed in the central part of the time series, from day 2 of acclimation to 15 min of de-acclimation (Figure S5A). Therefore, the corresponding 2,886 DEGs under HL, 3,121 under heat, and 5,433 observed under cold treatment (Table S4) were examined for their functional annotation into non-redundant Gene Ontology (GO) terms that were then grouped into main categories. Their protein products were assigned to a wide range of cellular compartments (extracellular, cytosol, organelles, especially chloroplasts, and nucleus) (Figure 3B). In the category "biological process," transcripts up-regulated under all treatments were mainly associated with abiotic stress responses, whereas HL and cold treatments specifically affected biotic stress responses and nucleic acid metabolism, respectively (Figure 3B). Moreover, transcripts associated with ribosome biogenesis were repressed under HL and heat, but those for protein synthesis and folding, as well as phosphorylation, increased in cold conditions. Down-regulated transcripts encoded proteins involved in responses to cytokinins (HL and heat) and auxin (cold). Under all treatments, transcripts for photosynthesis proteins were down-regulated (Figure 3B).

Moreover, global comparison of transcriptomes identified a set of 456 transcripts (Figure 3C) that changed, in the same direction, under all three conditions (Fisher's exact test, $p = 1.05 \times 10^{-34}$; Table S5). This indicates that all three environmental stimuli trigger a common transcriptional response, and analysis of the annotation of these proteins showed that chloroplast functions were overrepresented in this gene set (102 or 22% of genes, representing a 1.46-fold enrichment for GO term 0009507 "chloroplast"; Fisher's exact test, $p = 5.89 \times 10^{-5}$) (Table S6). It includes transcripts for several light-harvesting chlorophyll *a*/*b*-binding proteins (Lhcbs) and PSII subunits (Psb27, PsbO2, PsbQ1), and metabolic enzymes, along with proteins involved in redox reactions and heme and chlorophyll biosyntheses (Table S7). In general, most of these transcripts, except those involved in metabolism, were down-regulated during acclimation (Figure 3B and Table S6).

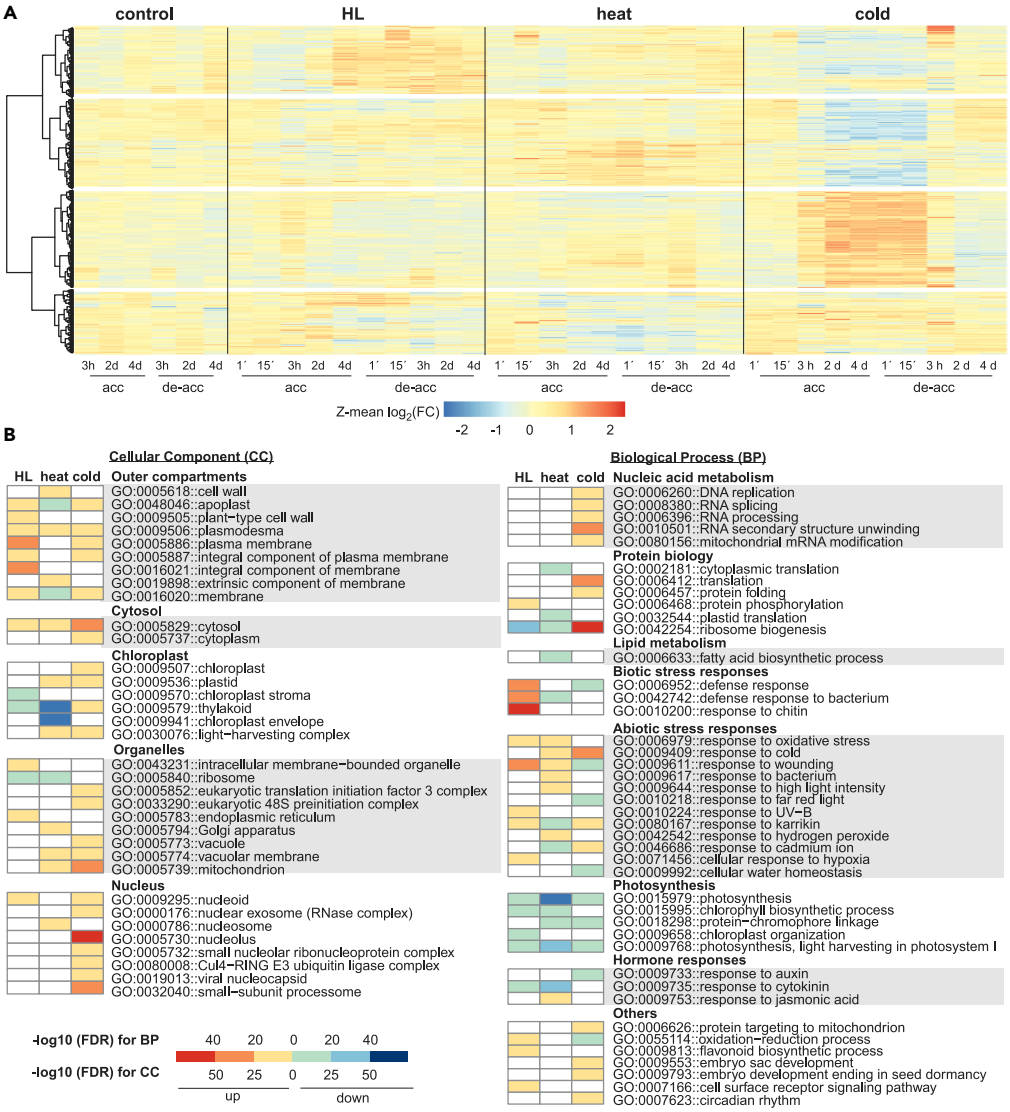

Figure 3. Changes in Transcript Accumulation during (De-)acclimation to High Light, Heat, and Cold

(A) Heatmaps based on Z-means of fold changes of DEGs. Major regulons were identified by clustering of Z-scores using Ward d2.

(B) Heatmaps illustrating non-redundant Gene Ontology (GO) term enrichment according to DAVID and REVIGO (Huang da et al., 2009a, 2009b; Supek et al., 2011). The color scale corresponds to the -$\log_{10}$ transformation of the FDR for the enrichment according to the Fisher's exact test. The regulatory trend of the transcripts in each bin (up or down) is indicated.

(C) Venn diagrams illustrating shared or unique DEGs, comprising total numbers (left panel, "total"), or only those that show the same (up-up or down-down, "same trend") or opposite (up-down or down-up, "opposite trend") polarities of regulation. Note that "same trend" and "opposite trend" sets do not always sum up to "total," because in several instances the polarity of regulation changed during the time course.

See also Figures S4 and S5.

In an attempt to identify transcription factors (TFs) tentatively mediating acclimation responses toward all examined conditions, the overlap between the list of 456 common genes and genes encoding TFs cataloged in the Database for Arabidopsis Transcription Factors (DATF; http://datf.cbi.pku.edu.cn) and in TAIR (https://www.arabidopsis.org) was determined. Overall, 41 TFs were identified (Table S5), among them the C-REPEAT/DRE BINDING FACTORs CBF1 and 2 and ETHYLENE RESPONSIVE ELEMENT BINDING FACTOR 6 (ERF6), which are established factors in the response to low temperatures (Zhao et al., 2016) and, in the case of ERF6, also HL (Vogel et al., 2014). In general, several TFs have been identified that were not related to acclimation responses before; they are members of diverse families including those of the bZIP-, MYC-, zinc-finger-, AP2/ERF-, Myb-, homeobox-, and NAC-type. At least two of them, MYC2 and G-BOX BINDING FACTOR 3 (GBF3), are binding to the G-box motif CACGTG, which is associated with various pathways, among them ambient temperature and light signaling (Ezer et al., 2017). Therefore, to obtain a deeper insight into putatively over-represented *cis*-acting elements, the 1,000-bp promoter sequences of the 456 common genes were scanned for 8-bp elements with the expectation maximization-based program Amadeus (Linhart et al., 2008). The highest similarity between queried motifs is defined by the lowest E-value, and the three identified over-represented motifs with the lowest E-value (Figure S6) were used to search the JASPAR 2020 plant database (http://jaspar.genereg.net/) (Fornes et al., 2020) for plant transcription factors known to bind to similar sequences. The motif with the lowest E-value found by JASPAR contained indeed the G-box motif (Figure S6). The second over-represented motif identified is predicted to be bound by MYB3, which represses phenylpropanoid biosynthesis gene expression (Zhou et al., 2017), whereas no known plant-associated element could be found for the third over-represented motif.

Surprisal Analysis of Transcriptome Changes during (De-)acclimation

To obtain insight into the molecular dynamics of the acclimation responses, we applied an unbiased thermodynamic maximal-entropy-based approach (surprisal analysis). In biological time series data, surprisal analysis can first identify the theoretical baseline state of minimal free energy of the system and then the constraints that prevent the system from reaching that baseline state. The contribution of the individual constraints is reflected by an associated time-dependent weight, the constraint potential (CP) (Gross et al., 2013; Kravchenko-Balasha et al., 2012; Levine, 1978, 1980; Remacle et al., 2010). Changes in sign of the CPs indicate whether the contribution of the input information (here transcript profile) to the constraint is inverted. Moreover, recovery of the CPs during de-acclimation to the original values for t = 0 of acclimation implies recovery of the underlying molecular dynamics.

For our transcriptome data, a stable baseline state for each condition was indeed obtained (Figure S7) and the datasets were therefore eligible for CP identification. All identified major CPs (CP1 to CP3) were found to change their signs in all three acclimation responses, whereas this tendency was less prominent for the minor CPs (CP4–CP10). Under HL conditions, the first major CP (HL-CP1) changed its sign at 4 days of acclimation and did not return to its original sign during de-acclimation. HL-CP2 and HL-CP3 changed their sign very early, at 15 min of acclimation, with HL-CP2 showing a tendency to return to the starting value at the end of the de-acclimation phase (Figure 4A). Heat-CP1 changed its sign at 2 days of acclimation and remained steady thereafter. As in the case of HL, heat-CP2 and heat-CP3 rapidly changed their sign (at 1 min and 3 h, respectively) and returned to values similar to the starting value during de-acclimation. Cold-CP1 was clearly reversible, changing its sign at 3 h of acclimation and again at 3 h of de-acclimation, to recover to initial levels. CP2 and CP3 under cold (de-)acclimation changed their sign three times (Figure 4A).

In subsets of transcripts, HL and heat provoke expression changes that are then maintained over the time span investigated here, possibly representing "memory" or "priming" effects (Crisp et al., 2017; Larkindale et al., 2005). A unique pattern was found for cold (de-)acclimation, which is the only condition under which the main acclimation state was fully reversed during the de-acclimation phase.

To investigate whether the constraints identified help to explain the physiological changes during acclimation and de-acclimation, we conducted partial least-squares (PLS) regression analysis of the three major CPs and the physiological parameters from Figure 1 (Figure 4B). A strong correlation in either direction on these plots indicates how well the physiological parameters can be explained using the CP time courses. This also allows one to rank the effects with respect to the constraint index as a proxy for energy investment, meaning primary effects are mainly explained by CP1, secondary effects by CP2, etc. For transcriptome

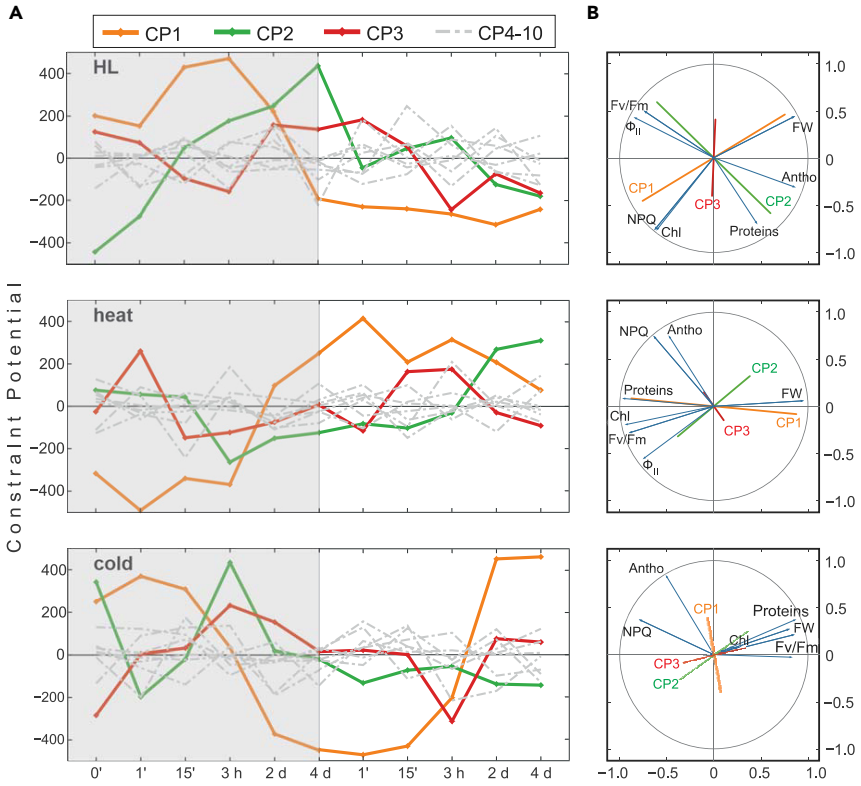

Figure 4. Surprisal Analysis of Transcriptome Changes during (De-)acclimation to High Light, Heat, and Cold

(A) Time course of the constraint potentials (CPs) derived from the transcriptome profiles of (de-)acclimation samples (high light [HL], heat, and cold). The minor constraints (4–10) are shown as gray lines; the acclimation phase is indicated by a gray square. Sign changes of CPs indicate reconfiguration of the underlying molecular dynamics.

(B) Circle correlation plots derived from partial least-squares regression analysis of CP1–3 of the time course shown in (A) and the physiological profiles depicted in Figure 1. Antho, anthocyanin content; Chl, chlorophyll content; FW, fresh weight; Φ_{II}, effective quantum yield of PSII; Fv/Fm, maximum quantum efficiency of PSII. Lines of CP1–CP3 in this plot were mirrored to reflect the fact that constraints contain positive and negative weights. Therefore, it is not possible to distinguish whether the effect was caused by positive or negative correlation.

See also Figure S7.

changes under HL, primary energy investment (HL-CP1) showed strong correlations with FW, NPQ, and chlorophyll content, but was almost perpendicular to all other physiological parameters, meaning there was no correlation with them (Figure 4B). However, Fv/Fm, Φ_{II}, and contents of anthocyanin and proteins correlated well with HL-CP2. Heat-CP1 correlated with FW, contents of proteins and chlorophyll, and Fv/Fm, and heat-CP2, with Φ_{II}. The only phenotypic parameter that correlated well with cold-CP1 was the anthocyanin content and, to a much lesser extent, NPQ. Cold-CP2 and, to a greater extent, cold-CP3 showed correlations with all other physiological parameters. Interestingly, PLS analysis also revealed that the physiological parameters FW and total protein content correlated positively only under cold (de-)acclimation.

Importantly, energy investment in these cases does not necessarily mean investment in the synthesis of these compounds, but relative investment in the creation of the respective pattern. Therefore, it can be concluded that different energy sources are used to sustain growth under HL and changing temperature conditions, with FW and chlorophyll content being common to HL and heat, and anthocyanin content characteristic for cold (de-)acclimation (Figure 4B).

Comparison of Topology and Dynamics of the Three Acclimation Responses

The transcriptome datasets were further analyzed in an unsupervised manner by the construction and subsequent analysis of conditional correlation networks. Briefly, co-expression matrices based on pairwise

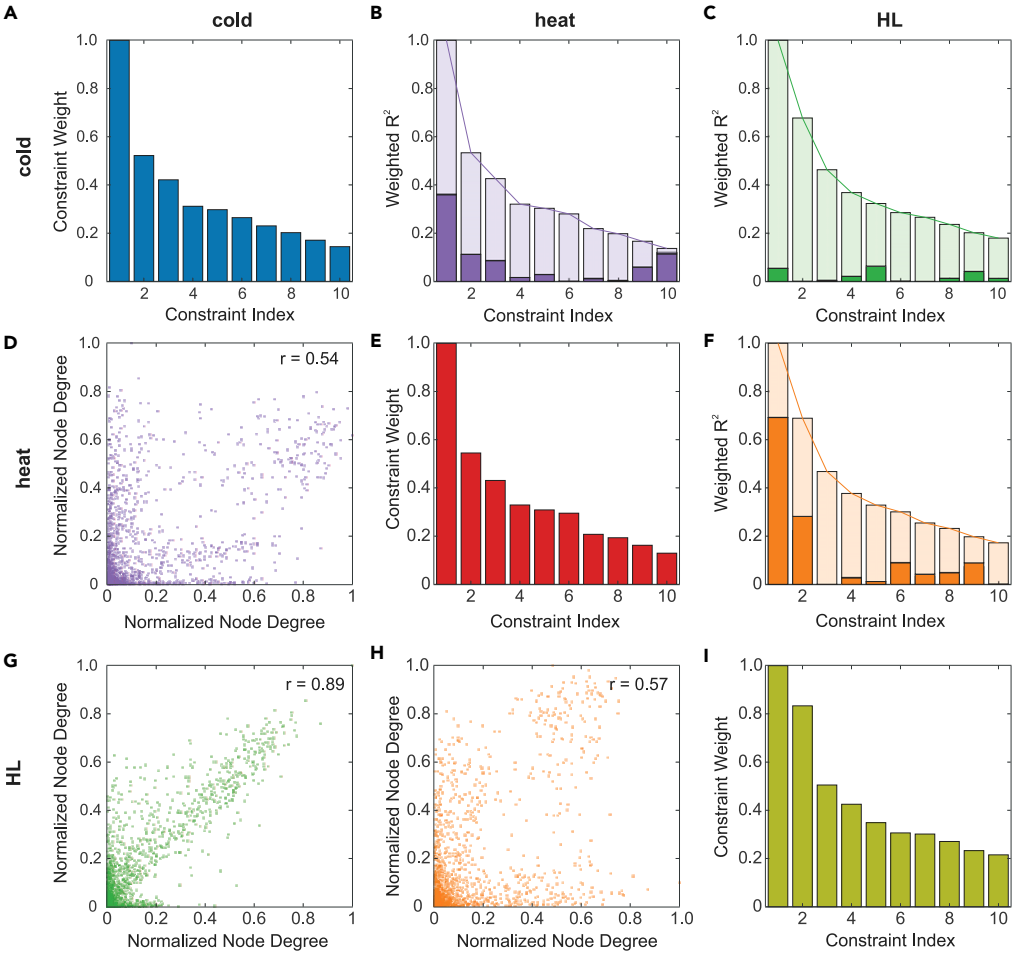

Figure 5. Commonalities and Differences between Acclimation Responses Revealed by Comparing Results of Conditional Network and Surprisal Analyses

Matrices showing correlations between constraint indices and weights, normalized node degrees, and weighted R^2 scores. Column and row headers indicate which conditions were compared with one another (blue = cold, red = heat, yellow = HL, purple = heat/cold, green = HL/cold, orange = heat/HL).

(A–I) (A, E, and I) Weights of the constraints determined by surprisal analysis for the three conditions. (B, C, and F) Weighted coefficients of determination (R^2) of linear regression analyses of constraint potential (CP) time courses determined by surprisal analysis for each constraint index (1–10) and depicted as column plots. Linear regression scores were calculated pairwise for CPs with the same index. R^2 was then weighted by the mean of the respective constraint weights of the two compared conditions shown on the diagonal. The open columns indicate the upper bound resulting from the weighting procedure. (D, G, and H) Correlation plots of normalized node degrees of the conditional network nodes. The Pearson correlation (r) is displayed for each plot.

See also Figures S8 and S9.

Pearson correlations among all detected transcripts for each condition were computed and mapped onto a literature-curated reference network to validate interactions and extract subnetworks that operate as conditional networks (Figure S8 and Table S8). The three transcriptional networks were similar in scale (comprising 4,600 to 5,600 nodes), although they differed in the number of connections (Table S8). The properties of the molecular topologies of these networks were then integrated with the data from CPs obtained by surprisal analysis. To this end, Pearson correlations among normalized degree distributions in each network were calculated. The networks under HL and cold were the most similar in their topology (r = 0.89), whereas more divergent patterns were obtained on comparing heat to either HL or cold networks (r = 0.57 and r = 0.54, respectively) (Figures 5D, 5G and 5H). A density plot of the Jaccard index was used as an additional measure of network similarity and showed the same pattern for the conditions, with the cold

A

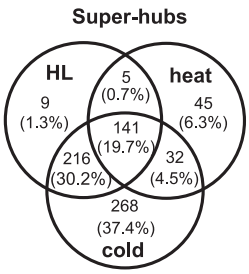

B

	GO term	Name	Counts	FDR
HL	GO:0006412	translation	186	1.44E-128
	GO:0042254	ribosome biogenesis	73	1.27E-83
	GO:0046686	response to cadmium ion	25	6.23E-05
	GO:0010501	RNA secondary structure unwinding	12	2.95E-05
heat	GO:0006412	translation	140	7.63E-111
	GO:0042254	ribosome biogenesis	47	4.83E-51
	GO:0009735	response to cytokinin	22	6.56E-12
	GO:0046686	response to cadmium ion	21	6.56E-06
	GO:0015979	photosynthesis	14	1.34E-05
	GO:0042742	defense response to bacterium	15	7.43E-03
	GO:0009409	response to cold	15	1.83E-02
cold	GO:0006412	translation	206	4.78E-98
	GO:0042254	ribosome biogenesis	86	5.81E-87
	GO:0046686	response to cadmium ion	46	1.77E-12
	GO:0010501	RNA secondary structure unwinding	21	4.82E-12
	GO:0009735	response to cytokinin	22	8.30E-04
	GO:0006360	transcription from RNA pol I promoter	8	8.41E-03
	GO:0009553	embryo sac development	12	3.26E-02

Figure 6. Analysis of Super-hubs in Conditional Networks for Transcripts

(A) Venn diagram depicting super-hubs (degree >100) common to the three networks.

(B) GO term enrichment of the identified super-hubs. The counts are provided, together with the FDR obtained with Fisher's exact test based on all nodes included in the networks.

versus HL comparison yielding the highest index (Figure S8). Therefore, similar features might be involved in the response pathways seen under HL and cold (de-)acclimation conditions.

To compare the dynamics of the three different (de-)acclimation responses as reflected by the CPs obtained by surprisal analysis, we performed pairwise linear regression on all CPs with the same index (1–10) in each treatment, using the intrinsic weighting scheme of surprisal analysis (Figures 5A, 5E, and 5I) to weight the resulting coefficients of determination (R^2). Interestingly, a pattern was observed that was inverted with respect to the topological comparison: although the pair HL and heat did not show strong correlation on the network level, they scored highly in the linear regression of CPs, especially for the first two CPs (weighted R^2 = 0.69 and 0.28, respectively) (Figure 5F). The same was true for heat and cold, albeit to a lesser extent (weighted R^2 = 0.36 and 0.11, respectively) (Figure 5B), whereas there was no notable correlation between HL and cold (Figure 5C).

Overall, therefore, HL and cold (de-)acclimation responses share similar regulatory networks, but display different dynamics. Conversely, the dynamics of the response to heat resembles that to HL (or cold), although different regulatory mechanisms seem to be at work.

Ribosomes Are Hubs of Acclimation

To identify the central components of acclimation responses, conditional networks were explored for hub composition. Hubs are highly connected nodes, providing information about sets of co-expressed nodes and therefore instances of coordinated transcriptional changes. If nodes with >100 edges are defined as super-hubs (Vandereyken et al., 2018), 371, 223, and 657 super-hubs were detected for the HL, heat, and cold networks, respectively (Tables S8 and S9). Interestingly, a significantly enriched fraction of 141 super-hubs (~20%; super exact test, $p = 1.04 \times 10^{-8}$) was shared among the three treatments. Moreover, 357 (216 + 141) super-hubs were common to HL and cold sets (~96% and ~55% of super-hubs under HL and cold, respectively; $p = 4.06 \times 10^{-71}$) (Figure 6A).

To gain insight into common responses to acclimation, these super-hubs were functionally annotated. To this end, significant GO terms (Fisher's exact test; FDR $\leq$0.05) were filtered for the non-redundant ones by employing REVIGO (Supek et al., 2011). Strikingly, GO enrichment analysis indicated that most of the super-hubs in each of the networks were related to the biological process categories "translation" (186 super-hubs under HL, 140 under heat, and 206 under cold, respectively) and "ribosome biogenesis" (73 under HL, 47 under heat, and 86 under cold). Most of these transcripts code for RPs (Figure 6B and Table S9).

To obtain a more detailed picture of the role of translation, and in particular the ribosome, in acclimation responses, the RP members of the HL, heat, and cold super-hubs (96, 108 and 207 members, respectively) were classified according to the subcellular localizations of their gene products using MapMan v.3.5.1

Subcellular Localization & Subunit	HL		Heat		Cold		Total
	# (Up/Down)	FE	# (Up/Down)	FE	# (Up/Down)	FE	
Cytosol							
40S	20 (0/20)	0.83	28 (2/26)	1.01	56 (56/0)	1.10	101
60S	41 (2/39)	1.04	39 (0/39)	0.86	110 (110/0)	1.32*	165
All	61 (2/59)	0.96	67 (2/65)	0.91	166 (166/0)	1.24*	266
Chloroplast							
30S	9 (0/9)	1.44	10 (0/10)	1.40	3 (2/1)	0.23*	26
50S	16 (0/16)	1.31	23 (0/23)	1.64*	9 (7/2)	0.35*	51
All	25 (0/25)	1.35*	33 (0/33)	1.56*	12 (9/3)	0.31*	77
Mitochondrion							
30S	–	0.00*	–	0.00*	–	0.00*	13
50S	1 (0/1)	0.60	–	0.00	5(5/0)	1.42	7
All	1 (0/1)	0.21*	0 (0/0)	0.00*	5 (5/0)	0.50*	20
Total							
	87 (2/85)		100 (2/98)		183 (180/3)		363

Table 1. Subcellular Localization, Numbers, and Enrichment of Ribosomal Proteins (RPs) Regulated at the Transcript Level during Acclimation

Transcriptional super-hubs for RPs were classified according to the subcellular localization of the corresponding ribosomal subunits based on MapMan (Thimm et al., 2004). The total number of transcripts in each category and the fold enrichment (FE) relative to the expected frequency of RPs are listed. The regulatory trend (up- or down-regulation) refers to changes in the transcript levels at 4 days of acclimation compared with the initial time point. Statistical significance of the enrichment according Fisher's two-sided exact test ($p \leq 0.05$) is indicated by an asterisk.

(Thimm et al., 2004). The HL, heat, and cold super-hubs included 26%, 30%, and 57% of all annotated transcripts coding for RPs with *bona fide* subcellular localization, and RPs from all three genetic compartments, cytosol, chloroplasts, and mitochondria were covered. Subtle compartment-specific enrichments of RPs were observed: cytosolic RPs appeared as over-represented super-hubs for cold and chloroplast-localized RPs were over-represented under HL and heat, but under-represented during cold, whereas mitochondrion-located RPs showed significant depletion under all conditions (Table 1). In contrast to these subtle changes, very clear trends were observed with respect to up- or down-regulation of RP-related super-hubs on day 4 of acclimation relative to t = 0 in the (de-)acclimation time series. The vast majority of ribosome-related transcripts that act as super-hubs tended to be down-regulated at the end of the acclimation phase (day 4) under HL and heat conditions, but up-regulated at the end of cold acclimation (Table 1). Heatmap analysis indicated that transcript levels of RPs were transiently up-regulated during HL and heat acclimation, and transiently down-regulated at the beginning of cold acclimation, before being down- (HL and heat) or up- (cold) regulated at the end of the acclimation phase (Figure S10 and Table S10).

Together, these observations indicate that modification of translation is a common and central element of acclimation responses, with very similar responses ensuing during HL and heat acclimation, and a different response occurring during cold acclimation.

DISCUSSION

A Comprehensive Analysis of (De-)acclimation to High Light, Heat, and Cold

In this work, we exposed *Arabidopsis* plants to moderate levels of light, heat, and cold stress that resulted in minimal, and largely reversible, physiological perturbations (see Figure 1). In contrast to previous studies (Suzuki et al., 2015; Vogel et al., 2014), we identified low numbers of DEGs after 1 and 15 min of HL (3 and 300; see Figure S5). This is attributable to our use of lower light dosages and LED sources, which did not

cause heat stress or trigger expression of heat-shock proteins. Moreover, we also avoided photoinhibition under our cold conditions by reducing light intensities (see Figure S1C). However, our acclimation treatments did lead to desynchronization of cells, as indicated by the perturbation of circadian gene expression and cell-cycle periodicity (see Figure S4).

Metabolome changes during acclimation comprised the accumulation of sugars and amino acids, especially under HL and cold treatments (see Table S2). At first glance, the accumulation of sugars appears to be in contradiction with the minimal FW losses observed under these two conditions and a transitory arrest of the photosynthetic light reactions during HL (see Figure 1). However, the increased content of central sugars such as maltose, sucrose, glucose, or fructose might result from increased starch turnover rather than increased photosynthesis. Under cold conditions, accumulation of sugars is not only aimed at providing energy but also to assure production of osmoprotectants like galactinol, raffinose, or *myo*-inositol. Similarly, the increased amino acid pools during the three conditions (see Figure 2) failed to correlate with changes in protein content (see Figure 1). This could imply that storage molecules, preferentially starch and/or lipids, rather than proteins are catabolized to meet the energetic demands of the acclimation response and maintain plant growth.

In general, HL and heat irreversibly altered metabolite profiles, whereas changes induced by cold treatment were readily reversible during de-acclimation (see Figure 2A). In contrast, transcriptome changes under HL and heat were only partially reversible (see Figures 3 and 4). Previous studies have observed similar patterns for both transcriptomes (Byun et al., 2014; Higashi et al., 2015; Huang et al., 2019; Zuther et al., 2015) and metabolites (Pagter et al., 2017; Vyse et al., 2019; Zuther et al., 2015). The (virtually) complete reversibility of the transcriptional response to cold may reflect the fact that the *Arabidopsis* ecotype Col-0 displays enhanced tolerance to low temperatures (Hannah et al., 2006; Kaplan et al., 2004; Yano et al., 2005).

As changes in metabolite profiles persisted during de-acclimation (see Figures 2 and S3), metabolites are obvious candidates for signals that prime plants to cope with future environmental challenges (Schwachtje et al., 2019; Serrano et al., 2019). We identified 7 metabolites (galactinol, phosphoenolpyruvate, glycine, tryptophan, lysine, alanine, and valine) whose concentrations increased under all conditions tested (Figure 2). Although accumulation of carbohydrates and organic acids, and their relocation between compartments, are well-known acclimation strategies (Dyson et al., 2015, 2016; Nägele and Heyer, 2013; Patzke et al., 2019; Pommerrenig et al., 2018), accumulation of amino acids during extended abiotic stress has been described only for cold-treated *Arabidopsis* plants (Espinoza et al., 2010; Kaplan et al., 2004; Lee et al., 2012; Pagter et al., 2017; Song et al., 2017) and deserves further investigation.

Our bioinformatic analysis suggested that HL and heat treatment induce similar temporal patterns of energy re-allocation. Conversely, topologies of conditional networks derived from co-expressed transcripts (see Figure 4) indicated that very similar regulatory pathways were triggered by HL and cold treatments. This implies that each acclimation response is characterized by a unique pattern of regulation that follows its own schedule.

Translation during (De-)acclimation

The existence of central elements that come into play under various types of adverse conditions regardless of the specific environmental input has been suggested in previous works (Kaplan et al., 2004; Kimura et al., 2003; Rocco et al., 2013). In our work, both unsupervised and supervised analyses of acclimation transcriptomes identified mRNAs for cytosolic and organellar RPs as shared and central factors in responses to diverse abiotic stresses (see Figure 6).

In mammalian cells, nucleoli and particularly ribosomes, are considered as hubs that integrate cellular responses to unfavorable conditions (Pfister, 2019; Warner and McIntosh, 2009; Yang et al., 2018). Under nucleolar stress ("ribostress"), RPs are exported to the cytosol and become pivotal components that help to trigger cell arrest or even apoptosis, depending on the level of stress (Pfister, 2019; Warner and McIntosh, 2009; Yang et al., 2018). A similar regulatory role for ribosomes during abiotic and biotic stresses is emerging in several plant species (Kim et al., 2004; Moin et al., 2016; Saez-Vasquez et al., 2000; Wang et al., 2013). A role of gene expression, in particular translation and the ribosome, in acclimation to abiotic environmental changes has been emerging in recent analyses of corresponding *Arabidopsis* mutants. In particular, various instances of impaired cold tolerances due to inactivation of chloroplast proteins involved

in translation have been described, including subunits (Rogalski et al., 2008; Wang et al., 2017; Zhang et al., 2016), associated proteins (Pulido et al., 2018), and biogenesis factors (Paieri et al., 2018; Reiter et al., 2020) of the plastid ribosome, translation initiation or elongation factors (Liu et al., 2010; Marino et al., 2019), and RNA-binding proteins (Kupsch et al., 2012). Furthermore, the cytosolic pre-18S rRNA processing factor RH7 is involved in cold tolerance (Huang et al., 2016), indicating that impairments in cytosolic translation can also affect cold tolerance. Fewer reports are available for an interplay of translation and tolerance to heat or HL, including enhanced heat sensitivity in the absence of the cytosolic translation initiation factor 5B (Zhang et al., 2017) or the plastid elongation factor Tu (Li et al., 2018), and HL sensitivity of seedlings lacking the cytosolic translation initiation factor 2a (Lokdarshi et al., 2020).

Why are transcripts for RPs mainly down-regulated at the end of the HL and heat acclimation phase, but up-regulated after cold acclimation? These trends coincide with previous studies employing alternative setups for HL, heat, and cold in *Arabidopsis* and other model organisms (Beine-Golovchuk et al., 2018; Guo et al., 2002; Guy, 1990; Kim et al., 2004; Moin et al., 2016; Thomashow, 1998). Down-regulation of RPs under high temperatures was initially supposed to reflect either increased mRNA instability or the need to restrict protein production, whereas up-regulation of RPs during cold stress was thought to maintain rates of protein synthesis under thermodynamically unfavorable conditions. However, a recent report has shown that mild oxidative stress affects the numbers of ribosomes in plants, but not overall translation efficiency (Salih et al., 2020), although plant genomes possess multiple gene copies for each RP (Barakat et al., 2001). This prompted the view that changes in RP expression under adverse conditions might be related to alterations of ribosomal composition required to adjust translation rates appropriately (Carroll et al., 2008; Giavalisco et al., 2005; Wang et al., 2013). Interestingly, in our experiments, neither the total protein content nor the pool of free amino acids in leaves decreased during acclimation (see Figures 1 and 2). Therefore, translation during (de-)acclimation is selectively reconfigured during HL/heat and cold, most likely involving changes in ribosome composition and/or readjustment of protein biosynthesis rate in subcellular compartments. A promising starting point to investigate a regulatory role of ribosomal activity, or more generally translational activity, during acclimation to other conditions than cold (for which such a function is well established) could be our list of nine genes encoding RNA-binding or ribosome-associated proteins, the mRNA levels of which changed during all conditions (see Table S5). Among them are *COLD, CIRCADIAN RHYTHM*, and *RNA BINDING 2* (*CCR2*)/*GLYCINE RICH PROTEIN 7* (*GRP7*) and AT2G27710, which encodes a 60S acidic RP. Interestingly, this protein was shown before to be regulated under cold conditions in a proteome analysis using differential in-gel electrophoresis (Amme et al., 2006).

Conclusion

Our work provides a holistic picture of three acclimation responses and suggests translation as the central process involved. Common up- or down-regulation of transcripts for RPs might reflect activation or repression of translation as a whole during acclimation, whereas regulatory factors that are transiently associated with the ribosome seem more likely to mediate central aspects of acclimation. Such modifications can be refined by taking advantage of promoters containing *cis*-elements being either specific to certain types of (de-)acclimation or being common to several responses (see Figure S6). In fact, our transcriptome kinetics is an ideal starting point for the identification of all kinds of (de-)acclimation-relevant promoters.

LIMITATIONS OF THE STUDY

Our conclusions are based on the analyses of large-scale omics data. Although the involvement of translational processes in cold acclimation is established (see Discussion section), future work is needed to validate the predicted central function of translation during heat and HL acclimation *in vivo*. Furthermore, targeted experiments are required to confirm the involvement of the proposed regulatory proteins and predicted *cis*-acting elements in the acclimation response. We used relatively young plants for our experiments. It will be of interest whether our conclusion can be transferred to (1) older plants and also (2) other plant species. As changes of most metabolites did not return to initial levels during heat and HL de-acclimation, future kinetics experiments should consider longer de-acclimation time periods.

Resource Availability

Lead Contact

Further information and requests for resources and reagents should be directed to and will be fulfilled by the Lead Contact, Dario Leister (leister@lmu.de).

Materials Availability

This study did not generate new unique reagents.

Data and Code Availability

The datasets generated during this study have been deposited to Gene Expression Omnibus (GEO; https://www.ncbi.nlm.nih.gov/geo/): GSE125950.

METHODS

All methods can be found in the accompanying Transparent Methods supplemental file.

SUPPLEMENTAL INFORMATION

Supplemental Information can be found online at https://doi.org/10.1016/j.isci.2020.101331.

ACKNOWLEDGMENTS

We thank Paul Hardy and Jose Muino for critical reading of the manuscript and the Deutsche Forschungsgemeinschaft (DFG) for funding (project TR175).

AUTHOR CONTRIBUTIONS

Conceptualization, D.L.; Methodology, K.S. and T.M.; Formal Analysis, A.G.-M., T.K., K.S., and T.M.; Investigation, A.G.-M., T.K., and M.L., Resources: D.L.; Writing: A.G.-M., T.K., and D.L. with input from all authors; Supervision: T.K. and D.L.; Funding acquisition: T.K., T.M., and D.L.

DECLARATION OF INTERESTS

The authors declare no competing interests.

Received: April 15, 2020
Revised: May 26, 2020
Accepted: June 28, 2020
Published: July 24, 2020

REFERENCES

Amme, S., Matros, A., Schlesier, B., and Mock, H.P. (2006). Proteome analysis of cold stress response in *Arabidopsis thaliana* using DIGE-technology. J. Exp. Bot. *57*, 1537–1546.

Anjum, N.A. (2015). Plant acclimation to environmental stress: a critical appraisal. Front. Plant Sci. *6*, 445.

Ashraf, M., Ahmad, M.S.A., Öztürk, M., and Aksoy, A. (2012). Crop improvement through different means: challenges and prospects. In Crop Production for Agricultural Improvement, M. Ashraf, M. Öztürk, M.S.A. Ahmad, and A. Aksoy, eds. (Springer Netherlands), pp. 1–15.

Barakat, A., Szick-Miranda, K., Chang, I.F., Guyot, R., Blanc, G., Cooke, R., Delseny, M., and Bailey-Serres, J. (2001). The organization of cytoplasmic ribosomal protein genes in the Arabidopsis genome. Plant Physiol. *127*, 398–415.

Beine-Golovchuk, O., Firmino, A.A.P., Dabrowska, A., Schmidt, S., Erban, A., Walther, D., Zuther, E., Hincha, D.K., and Kopka, J. (2018). Plant temperature acclimation and growth rely on cytosolic ribosome biogenesis factor homologs. Plant Physiol. *176*, 2251–2276.

Buchanan, B.B., Gruissem, W., and Jones, R.L. (2000). Biochemistry & Molecular Biology of Plants (American Society of Plant Physiologists).

Byun, Y.J., Koo, M.Y., Joo, H.J., Ha-Lee, Y.M., and Lee, D.H. (2014). Comparative analysis of gene expression under cold acclimation, deacclimation and reacclimation in Arabidopsis. Physiol. Plant *152*, 256–274.

Caldana, C., Degenkolbe, T., Cuadros-Inostroza, A., Klie, S., Sulpice, R., Leisse, A., Steinhauser, D., Fernie, A.R., Willmitzer, L., and Hannah, M.A. (2011). High-density kinetic analysis of the metabolomic and transcriptomic response of Arabidopsis to eight environmental conditions. Plant J. *67*, 869–884.

Carrera, D.Á., Oddsson, S., Grossmann, J., Trachsel, C., and Streb, S. (2017). Comparative proteomic analysis of plant acclimation to six different long-term environmental changes. Plant Cell Physiol. *59*, 510–526.

Carroll, A.J., Heazlewood, J.L., Ito, J., and Millar, A.H. (2008). Analysis of the Arabidopsis cytosolic ribosome proteome provides detailed insights into its components and their post-translational modification. Mol. Cell Proteomics *7*, 347–369.

Carvalho, F.E., Ware, M.A., and Ruban, A.V. (2015). Quantifying the dynamics of light tolerance in Arabidopsis plants during ontogenesis. Plant Cell Environ. *38*, 2603–2617.

Cerny, M., Jedelsky, P.L., Novak, J., Schlosser, A., and Brzobohaty, B. (2014). Cytokinin modulates proteomic, transcriptomic and growth responses to temperature shocks in Arabidopsis. Plant Cell Environ. *37*, 1641–1655.

Chia, D.W., Yoder, T.J., Reiter, W.D., and Gibson, S.I. (2000). Fumaric acid: an overlooked form of fixed carbon in Arabidopsis and other plant species. Planta *211*, 743–751.

Crawford, A.J., McLachlan, D.H., Hetherington, A.M., and Franklin, K.A. (2012). High temperature exposure increases plant cooling capacity. Curr. Biol. *22*, R396–R397.

Crisp, P.A., Ganguly, D.R., Smith, A.B., Murray, K.D., Estavillo, G.M., Searle, I., Ford, E., Bogdanovic, O., Lister, R., Borevitz, J.O., et al. (2017). Rapid recovery gene downregulation during excess-light stress and recovery in Arabidopsis. Plant Cell *29*, 1836–1863.

Dyson, B.C., Allwood, J.W., Feil, R., Xu, Y., Miller, M., Bowsher, C.G., Goodacre, R., Lunn, J.E., and Johnson, G.N. (2015). Acclimation of metabolism to light in *Arabidopsis thaliana*: the glucose 6-phosphate/phosphate translocator GPT2 directs metabolic acclimation. Plant Cell Environ. *38*, 1404–1417.

Dyson, B.C., Miller, M.A., Feil, R., Rattray, N., Bowsher, C.G., Goodacre, R., Lunn, J.E., and Johnson, G.N. (2016). FUM2, a cytosolic fumarase, is essential for acclimation to low temperature in *Arabidopsis thaliana*. Plant Physiol. *172*, 118–127.

Espinoza, C., Degenkolbe, T., Caldana, C., Zuther, E., Leisse, A., Willmitzer, L., Hincha, D.K., and Hannah, M.A. (2010). Interaction with diurnal and circadian regulation results in dynamic metabolic and transcriptional changes during cold acclimation in Arabidopsis. PLoS One *5*, e14101.

Ezer, D., Shepherd, S.J.K., Brestovitsky, A., Dickinson, P., Cortijo, S., Charoensawan, V., Box, M.S., Biswas, S., Jaeger, K.E., and Wigge, P.A. (2017). The G-Box transcriptional regulatory code in Arabidopsis. Plant Physiol. *175*, 628–640.

Fornes, O., Castro-Mondragon, J.A., Khan, A., van der Lee, R., Zhang, X., Richmond, P.A., Modi, B.P., Correard, S., Gheorghe, M., Baranasic, D., et al. (2020). Jaspar 2020: update of the open-access database of transcription factor binding profiles. Nucleic Acids Res. *48*, D87–D92.

Fowler, S., and Thomashow, M.F. (2002). Arabidopsis transcriptome profiling indicates that multiple regulatory pathways are activated during cold acclimation in addition to the CBF cold response pathway. Plant Cell *14*, 1675–1690.

Foyer, C.H., Bloom, A.J., Queval, G., and Noctor, G. (2009). Photorespiratory metabolism: genes, mutants, energetics, and redox signaling. Annu. Rev. Plant Biol. *60*, 455–484.

Garcia-Molina, A., and Leister, D. (2020). Accelerated relaxation of photoprotection impairs biomass accumulation in Arabidopsis. Nat. Plants *6*, 9–12.

Giavalisco, P., Wilson, D., Kreitler, T., Lehrach, H., Klose, J., Gobom, J., and Fucini, P. (2005). High heterogeneity within the ribosomal proteins of the *Arabidopsis thaliana* 80S ribosome. Plant Mol. Biol. *57*, 577–591.

Gross, A., Li, C.M., Remacle, F., and Levine, R.D. (2013). Free energy rhythms in *Saccharomyces cerevisiae*: a dynamic perspective with implications for ribosomal biogenesis. Biochemistry *52*, 1641–1648.

Grotewold, E. (2006). The genetics and biochemistry of floral pigments. Annu. Rev. Plant Biol. *57*, 761–780.

Guo, Y., Xiong, L., Ishitani, M., and Zhu, J.-K. (2002). An *Arabidopsis* mutation in translation elongation factor 2 causes superinduction of *CBF/DREB1* transcription factor genes but blocks the induction of their downstream targets under low temperatures. Proc. Natl. Acad. Sci. U S A *99*, 7786.

Guy, C., Haskell, D., Li, Q.-B., and Zhang, C. (1997). Molecular chaperones: do they have a role in cold stress responses of plants? In Plant Cold Hardiness: Molecular Biology, Biochemistry, and Physiology, P.H. Li and T.H.H. Chen, eds. (Springer US), pp. 109–129.

Guy, C.L. (1990). Cold acclimation and freezing stress tolerance: role of protein metabolism. Annu. Rev. Plant Physiol. Plant Mol. Biol. *41*, 187–223.

Hannah, M.A., Heyer, A.G., and Hincha, D.K. (2005). A global survey of gene regulation during cold acclimation in *Arabidopsis thaliana*. PLoS Genet. *1*, e26.

Hannah, M.A., Wiese, D., Freund, S., Fiehn, O., Heyer, A.G., and Hincha, D.K. (2006). Natural genetic variation of freezing tolerance in Arabidopsis. Plant Physiol. *142*, 98–112.

Harvaux, M., and Kloppstech, K. (2001). The protective functions of carotenoid and flavonoid pigments against excess visible radiation at chilling temperature investigated in Arabidopsis *npq* and *tt* mutants. Planta *213*, 953–966.

Higashi, Y., Okazaki, Y., Myouga, F., Shinozaki, K., and Saito, K. (2015). Landscape of the lipidome and transcriptome under heat stress in *Arabidopsis thaliana*. Sci. Rep. *5*, 10533.

Hoermiller, , II, Naegele, T., Augustin, H., Stutz, S., Weckwerth, W., and Heyer, A.G. (2017). Subcellular reprogramming of metabolism during cold acclimation in *Arabidopsis thaliana*. Plant Cell Environ. *40*, 602–610.

Huang, C.K., Shen, Y.L., Huang, L.F., Wu, S.J., Yeh, C.H., and Lu, C.A. (2016). The DEAD-box RNA helicase AtRH7/PRH75 participates in pre-rRNA processing, plant development and cold tolerance in Arabidopsis. Plant Cell Physiol. *57*, 174–191.

Huang da, W., Sherman, B.T., and Lempicki, R.A. (2009a). Bioinformatics enrichment tools: paths toward the comprehensive functional analysis of large gene lists. Nucleic Acids Res. *37*, 1–13.

Huang da, W., Sherman, B.T., and Lempicki, R.A. (2009b). Systematic and integrative analysis of large gene lists using DAVID bioinformatics resources. Nat. Protoc. *4*, 44–57.

Huang, J., Zhao, X., and Chory, J. (2019). The Arabidopsis transcriptome responds specifically and dynamically to high light stress. Cell Rep. *29*, 4186–4199.e3.

Juszczak, I., Cvetkovic, J., Zuther, E., Hincha, D.K., and Baier, M. (2016). Natural variation of cold deacclimation correlates with variation of cold-acclimation of the plastid antioxidant system in *Arabidopsis thaliana* accessions. Front. Plant Sci. *7*, 305.

Kaplan, F., Kopka, J., Haskell, D.W., Zhao, W., Schiller, K.C., Gatzke, N., Sung, D.Y., and Guy, C.L. (2004). Exploring the temperature-stress metabolome of Arabidopsis. Plant Physiol. *136*, 4159–4168.

Kaplan, F., Kopka, J., Sung, D.Y., Zhao, W., Popp, M., Porat, R., and Guy, C.L. (2007). Transcript and metabolite profiling during cold acclimation of Arabidopsis reveals an intricate relationship of cold-regulated gene expression with modifications in metabolite content. Plant J. *50*, 967–981.

Karpinski, S., Szechynska-Hebda, M., Wituszynska, W., and Burdiak, P. (2013). Light acclimation, retrograde signalling, cell death and immune defences in plants. Plant Cell Environ. *36*, 736–744.

Kim, K.Y., Park, S.W., Chung, Y.S., Chung, C.H., Kim, J.I., and Lee, J.H. (2004). Molecular cloning of low-temperature-inducible ribosomal proteins from soybean. J. Exp. Bot. *55*, 1153–1155.

Kimura, M., Yamamoto, Y.Y., Seki, M., Sakurai, T., Sato, M., Abe, T., Yoshida, S., Manabe, K., Shinozaki, K., and Matsui, M. (2003). Identification of Arabidopsis genes regulated by high light-stress using cDNA microarray. Photochem. Photobiol. *77*, 226–233.

Kravchenko-Balasha, N., Levitzki, A., Goldstein, A., Rotter, V., Gross, A., Remacle, F., and Levine, R.D. (2012). On a fundamental structure of gene networks in living cells. Proc. Natl. Acad. Sci. U S A *109*, 4702.

Kromdijk, J., Głowacka, K., Leonelli, L., Gabilly, S.T., Iwai, M., Niyogi, K.K., and Long, S.P. (2016). Improving photosynthesis and crop productivity by accelerating recovery from photoprotection. Science *354*, 857–861.

Kupsch, C., Ruwe, H., Gusewski, S., Tillich, M., Small, I., and Schmitz-Linneweber, C. (2012). Arabidopsis chloroplast RNA binding proteins CP31A and CP29A associate with large transcript pools and confer cold stress tolerance by influencing multiple chloroplast RNA processing steps. Plant Cell *24*, 4266–4280.

Larkindale, J., Hall, J.D., Knight, M.R., and Vierling, E. (2005). Heat stress phenotypes of Arabidopsis mutants implicate multiple signaling pathways in the acquisition of thermotolerance. Plant Physiol. *138*, 882.

Larkindale, J., and Vierling, E. (2008). Core genome responses involved in acclimation to high temperature. Plant Physiol. *146*, 748–761.

Lee, Y.P., Babakov, A., de Boer, B., Zuther, E., and Hincha, D.K. (2012). Comparison of freezing tolerance, compatible solutes and polyamines in geographically diverse collections of *Thellungiella* sp. and *Arabidopsis thaliana* accessions. BMC Plant Biol. *12*, 131.

Levine, R.D. (1978). Information theory approach to molecular reaction dynamics. Ann. Rev. Phys. Chem. *29*, 59–92.

Levine, R.D. (1980). An information theoretical approach to inversion problems. J. Phys. A Math. Gen. *13*, 91–108.

Li, X., Cai, C., Wang, Z., Fan, B., Zhu, C., and Chen, Z. (2018). Plastid translation elongation factor Tu is prone to heat-induced aggregation despite its critical role in plant heat tolerance. Plant Physiol. *176*, 3027–3045.

Linhart, C., Halperin, Y., and Shamir, R. (2008). Transcription factor and microRNA motif discovery: the Amadeus platform and a compendium of metazoan target sets. Genome Res. *18*, 1180–1189.

Liu, X., Rodermel, S.R., and Yu, F. (2010). A *var2* leaf variegation suppressor locus, SUPPRESSOR OF VARIEGATION3, encodes a putative chloroplast translation elongation factor that is important for chloroplast development in the cold. BMC Plant Biol. *10*, 287.

Lobell, D.B., and Gourdji, S.M. (2012). The influence of climate change on global crop productivity. Plant Physiol. *160*, 1686–1697.

Lokdarshi, A., Guan, J., Urquidi Camacho, R.A., Cho, S.K., Morgan, P.W., Leonard, M., Shimono, M., Day, B., and von Arnim, A.G. (2020). Light activates the translational regulatory kinase GCN2 via reactive oxygen species emanating from the chloroplast. Plant Cell *32*, 1161–1178.

Marino, G., Naranjo, B., Wang, J., Penzler, J.F., Kleine, T., and Leister, D. (2019). Relationship of GUN1 to FUG1 in chloroplast protein homeostasis. Plant J. *99*, 521–535.

Miki, Y., Takahashi, D., Kawamura, Y., and Uemura, M. (2018). Temporal proteomics of Arabidopsis plasma membrane during cold- and de-acclimation. J. Proteomics *197*, 71–81.

Moin, M., Bakshi, A., Saha, A., Dutta, M., Madhav, S.M., and Kirti, P.B. (2016). Rice ribosomal protein large subunit genes and their spatio-temporal and stress regulation. Front. Plant Sci. *7*, 1284.

Mueller, S.P., Krause, D.M., Mueller, M.J., and Fekete, A. (2015). Accumulation of extra-chloroplastic triacylglycerols in Arabidopsis seedlings during heat acclimation. J. Exp. Bot. *66*, 4517–4526.

Mullineaux, P., and Karpinski, S. (2002). Signal transduction in response to excess light: getting out of the chloroplast. Curr. Opin. Plant Biol. *5*, 43–48.

Nägele, T., and Heyer, A.G. (2013). Approximating subcellular organisation of carbohydrate metabolism during cold acclimation in different natural accessions of *Arabidopsis thaliana*. New Phytol. *198*, 777–787.

Nakaminami, K., Matsui, A., Nakagami, H., Minami, A., Nomura, Y., Tanaka, M., Morosawa, T., Ishida, J., Takahashi, S., Uemura, M., et al. (2014). Analysis of differential expression patterns of mRNA and protein during cold-acclimation and de-acclimation in Arabidopsis. Mol. Cell Proteomics *13*, 3602–3611.

Nishizawa, A., Yabuta, Y., and Shigeoka, S. (2008). Galactinol and raffinose constitute a novel function to protect plants from oxidative damage. Plant Physiol. *147*, 1251–1263.

Noctor, G., Queval, G., Mhamdi, A., Chaouch, S., and Foyer, C.H. (2011). Glutathione. Arabidopsis Book *9*, e0142.

Pagter, M., Alpers, J., Erban, A., Kopka, J., Zuther, E., and Hincha, D.K. (2017). Rapid transcriptional and metabolic regulation of the deacclimation process in cold acclimated *Arabidopsis thaliana*. BMC Genomics *18*, 731.

Paieri, F., Tadini, L., Manavski, N., Kleine, T., Ferrari, R., Morandini, P., Pesaresi, P., Meurer, J., and Leister, D. (2018). The DEAD-box RNA helicase RH50 is a 23S-4.5S rRNA maturation factor that functionally overlaps with the plastid signaling factor GUN1. Plant Physiol. *176*, 634–648.

Panikulangara, T.J., Eggers-Schumacher, G., Wunderlich, M., Stransky, H., and Schoffl, F. (2004). Galactinol synthase1. A novel heat shock factor target gene responsible for heat-induced synthesis of raffinose family oligosaccharides in Arabidopsis. Plant Physiol. *136*, 3148–3158.

Park, C.J., and Seo, Y.S. (2015). Heat shock proteins: a review of the molecular chaperones for plant immunity. Plant Pathol. J. *31*, 323–333.

Patzke, K., Prananingrum, P., Klemens, P.A.W., Trentmann, O., Rodrigues, C.M., Keller, I., Fernie, A.R., Geigenberger, P., Bölter, B., Lehmann, M., et al. (2019). The plastidic sugar transporter pSuT influences flowering and affects cold responses. Plant Physiol. *179*, 569–587.

Pfister, A.S. (2019). Emerging role of the nucleolar stress response in autophagy. Front. Cell Neurosci. *13*, 156.

Pinnola, A., and Bassi, R. (2018). Molecular mechanisms involved in plant photoprotection. Biochem. Soc. Trans. *46*, 467–482.

Pommerrenig, B., Ludewig, F., Cvetkovic, J., Trentmann, O., Klemens, P.A.W., and Neuhaus, H.E. (2018). In concert: orchestrated changes in carbohydrate homeostasis are critical for plant abiotic stress tolerance. Plant Cell Physiol. *59*, 1290–1299.

Pulido, P., Zagari, N., Manavski, N., Gawronski, P., Matthes, A., Scharff, L.B., Meurer, J., and Leister, D. (2018). CHLOROPLAST RIBOSOME ASSOCIATED supports translation under stress and interacts with the ribosomal 30S subunit. Plant Physiol. *177*, 1539–1554.

Reddy, P.P. (2015). Impacts of climate change on agriculture. In Climate Resilient Agriculture for Ensuring Food Security (Springer India), pp. 43–90.

Reiter, B., Vamvaka, E., Marino, G., Kleine, T., Jahns, P., Bolle, C., Leister, D., and Ruhle, T. (2020). The Arabidopsis protein CGL20 is required for plastid 50S ribosome biogenesis. Plant Physiol. *182*, 1222–1238.

Remacle, F., Kravchenko-Balasha, N., Levitzki, A., and Levine, R.D. (2010). Information-theoretic analysis of phenotype changes in early stages of carcinogenesis. Proc. Natl. Acad. Sci. U S A *107*, 10324.

Rocco, M., Arena, S., Renzone, G., Scippa, G.S., Lomaglio, T., Verrillo, F., Scaloni, A., and Marra, M. (2013). Proteomic analysis of temperature stress-responsive proteins in *Arabidopsis thaliana* rosette leaves. Mol. Biosyst. *9*, 1257–1267.

Rogalski, M., Schottler, M.A., Thiele, W., Schulze, W.X., and Bock, R. (2008). Rpl33, a nonessential plastid-encoded ribosomal protein in tobacco, is required under cold stress conditions. Plant Cell *20*, 2221–2237.

Rossel, J.B., Wilson, I.W., and Pogson, B.J. (2002). Global changes in gene expression in response to high light in Arabidopsis. Plant Physiol. *130*, 1109–1120.

Ruban, A.V. (2016). Nonphotochemical chlorophyll fluorescence quenching: mechanism and effectiveness in protecting plants from photodamage. Plant Physiol. *170*, 1903–1916.

Saez-Vasquez, J., Gallois, P., and Delseny, M. (2000). Accumulation and nuclear targeting of BnC24, a Brassica napus ribosomal protein corresponding to a mRNA accumulating in response to cold treatment. Plant Sci. *156*, 35–46.

Salih, K.J., Duncan, O., Li, L., O'Leary, B., Fenske, R., Troesch, J., and Millar, A.H. (2020). Impact of oxidative stress on the function, abundance and turnover of the Arabidopsis 80S cytosolic ribosome. Plant J. https://doi.org/10.1111/tpj.14713.

Sanchez-Bermejo, E., Zhu, W., Tasset, C., Eimer, H., Sureshkumar, S., Singh, R., Sundaramoorthi, V., Colling, L., and Balasubramanian, S. (2015). Genetic architecture of natural variation in thermal responses of Arabidopsis. Plant Physiol. *169*, 647.

Schmitz, J., Heinrichs, L., Scossa, F., Fernie, A.R., Oelze, M.L., Dietz, K.J., Rothbart, M., Grimm, B., Flugge, U.I., and Hausler, R.E. (2014). The essential role of sugar metabolism in the acclimation response of *Arabidopsis thaliana* to high light intensities. J. Exp. Bot. *65*, 1619–1636.

Schulz, E., Tohge, T., Zuther, E., Fernie, A.R., and Hincha, D.K. (2016). Flavonoids are determinants of freezing tolerance and cold acclimation in *Arabidopsis thaliana*. Sci. Rep. *6*, 34027.

Schwachtje, J., Whitcomb, S.J., Firmino, A.A.P., Zuther, E., Hincha, D.K., and Kopka, J. (2019). Induced, imprinted, and primed responses to changing environments: does metabolism store and process information? Front. Plant Sci. *10*, 106.

Serrano, N., Ling, Y., Bahieldin, A., and Mahfouz, M.M. (2019). Thermopriming reprograms metabolic homeostasis to confer heat tolerance. Sci. Rep. *9*, 181.

Song, Y., Liu, L., Wei, Y., Li, G., Yue, X., and An, L. (2017). Metabolite profiling of *adh1* mutant response to cold stress in Arabidopsis. Front. Plant Sci. *7*, 2072.

Speiser, A., Haberland, S., Watanabe, M., Wirtz, M., Dietz, K.-J., Saito, K., and Hell, R. (2015). The significance of cysteine synthesis for acclimation to high light conditions. Front. Plant Sci. *5*, 776.

Supek, F., Bosnjak, M., Skunca, N., and Smuc, T. (2011). REVIGO summarizes and visualizes long lists of gene ontology terms. PLoS One *6*, e21800.

Suzuki, N., Devireddy, A.R., Inupakutika, M.A., Baxter, A., Miller, G., Song, L., Shulaev, E., Azad, R.K., Shulaev, V., and Mittler, R. (2015). Ultra-fast alterations in mRNA levels uncover multiple players in light stress acclimation in plants. Plant J. *84*, 760–772.

Thimm, O., Blasing, O., Gibon, Y., Nagel, A., Meyer, S., Kruger, P., Selbig, J., Muller, L.A., Rhee, S.Y., and Stitt, M. (2004). MAPMAN: a user-driven tool to display genomics data sets onto diagrams of metabolic pathways and other biological processes. Plant J. *37*, 914–939.

Thomashow, M.F. (1998). Role of cold-responsive genes in plant freezing tolerance. Plant Physiol. *118*, 1.

Vandereyken, K., Van Leene, J., De Coninck, B., and Cammue, B.P.A. (2018). Hub protein controversy: taking a closer look at plant stress response hubs. Front. Plant Sci. *9*, 694.

Vogel, M.O., Moore, M., Konig, K., Pecher, P., Alsharafa, K., Lee, J., and Dietz, K.J. (2014). Fast retrograde signaling in response to high light involves metabolite export, MITOGEN-ACTIVATED PROTEIN KINASE6, and AP2/ERF

transcription factors in Arabidopsis. Plant Cell *26*, 1151–1165.

Vyse, K., Pagter, M., Zuther, E., and Hincha, D.K. (2019). Deacclimation after cold acclimation—a crucial, but widely neglected part of plant winter survival. J. Exp. Bot. *70*, 4595–4604.

Wang, J., Lan, P., Gao, H., Zheng, L., Li, W., and Schmidt, W. (2013). Expression changes of ribosomal proteins in phosphate- and iron-deficient Arabidopsis roots predict stress-specific alterations in ribosome composition. BMC Genomics *14*, 783.

Wang, L., Ma, K.B., Lu, Z.G., Ren, S.X., Jiang, H.R., Cui, J.W., Chen, G., Teng, N.J., Lam, H.M., and Jin, B. (2020). Differential physiological, transcriptomic and metabolomic responses of Arabidopsis leaves under prolonged warming and heat shock. BMC Plant Biol. *20*, 86.

Wang, M., Zhao, Y., and Zhang, B. (2015). Efficient test and visualization of multi-set intersections. Sci. Rep. *5*, 16923.

Wang, W., Vinocur, B., Shoseyov, O., and Altman, A. (2004). Role of plant heat-shock proteins and molecular chaperones in the abiotic stress response. Trends Plant Sci. *9*, 244–252.

Wang, W.J., Zheng, K.L., Gong, X.D., Xu, J.L., Huang, J.R., Lin, D.Z., and Dong, Y.J. (2017). The rice TCD11 encoding plastid ribosomal protein S6 is essential for chloroplast development at low temperature. Plant Sci. *259*, 1–11.

Warner, J.R., and McIntosh, K.B. (2009). How common are extraribosomal functions of ribosomal proteins? Mol. Cell *34*, 3–11.

Yamori, W. (2016). Photosynthetic response to fluctuating environments and photoprotective strategies under abiotic stress. J. Plant Res. *129*, 379–395.

Yang, K., Yang, J., and Yi, J. (2018). Nucleolar stress: hallmarks, sensing mechanism and diseases. Cell Stress *2*, 125–140.

Yano, R., Nakamura, M., Yoneyama, T., and Nishida, I. (2005). Starch-related α-glucan/water dikinase is involved in the cold-induced development of freezing tolerance in Arabidopsis. Plant Physiol. *138*, 837–846.

Zandalinas, S.I., Sengupta, S., Burks, D., Azad, R.K., and Mittler, R. (2019). Identification and characterization of a core set of ROS wave-associated transcripts involved in the systemic acquired acclimation response of Arabidopsis to excess light. Plant J. *98*, 126–141.

Zhang, J., Yuan, H., Yang, Y., Fish, T., Lyi, S.M., Thannhauser, T.W., Zhang, L., and Li, L. (2016). Plastid ribosomal protein S5 is involved in photosynthesis, plant development, and cold stress tolerance in Arabidopsis. J. Exp. Bot. *67*, 2731–2744.

Zhang, L., Liu, X., Gaikwad, K., Kou, X., Wang, F., Tian, X., Xin, M., Ni, Z., Sun, Q., Peng, H., et al. (2017). Mutations in eIF5B confer thermosensitive and pleiotropic phenotypes via translation defects in *Arabidopsis thaliana*. Plant Cell *29*, 1952–1969.

Zhang, R., Wise, R.R., Struck, K.R., and Sharkey, T.D. (2010). Moderate heat stress of *Arabidopsis thaliana* leaves causes chloroplast swelling and plastoglobule formation. Photosynth Res. *105*, 123–134.

Zhao, C., Wang, P., Si, T., Hsu, C.C., Wang, L., Zayed, O., Yu, Z., Zhu, Y., Dong, J., Tao, W.A., et al. (2017). MAP kinase cascades regulate the cold response by modulating ICE1 protein stability. Dev. Cell *43*, 618–629.e5.

Zhao, C., Zhang, Z., Xie, S., Si, T., Li, Y., and Zhu, J.K. (2016). Mutational evidence for the critical role of CBF transcription factors in cold acclimation in Arabidopsis. Plant Physiol. *171*, 2744–2759.

Zhou, M., Zhang, K., Sun, Z., Yan, M., Chen, C., Zhang, X., Tang, Y., and Wu, Y. (2017). LNK1 and LNK2 corepressors interact with the MYB3 transcription factor in phenylpropanoid biosynthesis. Plant Physiol. *174*, 1348–1358.

Zuther, E., Juszczak, I., Lee, Y.P., Baier, M., and Hincha, D.K. (2015). Time-dependent deacclimation after cold acclimation in *Arabidopsis thaliana* accessions. Sci. Rep. *5*, 12199.

Zuther, E., Schaarschmidt, S., Fischer, A., Erban, A., Pagter, M., Mubeen, U., Giavalisco, P., Kopka, J., Sprenger, H., and Hincha, D.K. (2019). Molecular signatures associated with increased freezing tolerance due to low temperature memory in Arabidopsis. Plant Cell Environ. *42*, 854–873.

iScience, Volume *23*

Supplemental Information

Translational Components Contribute to Acclimation Responses to High Light, Heat, and Cold in *Arabidopsis*

Antoni Garcia-Molina, Tatjana Kleine, Kevin Schneider, Timo Mühlhaus, Martin Lehmann, and Dario Leister

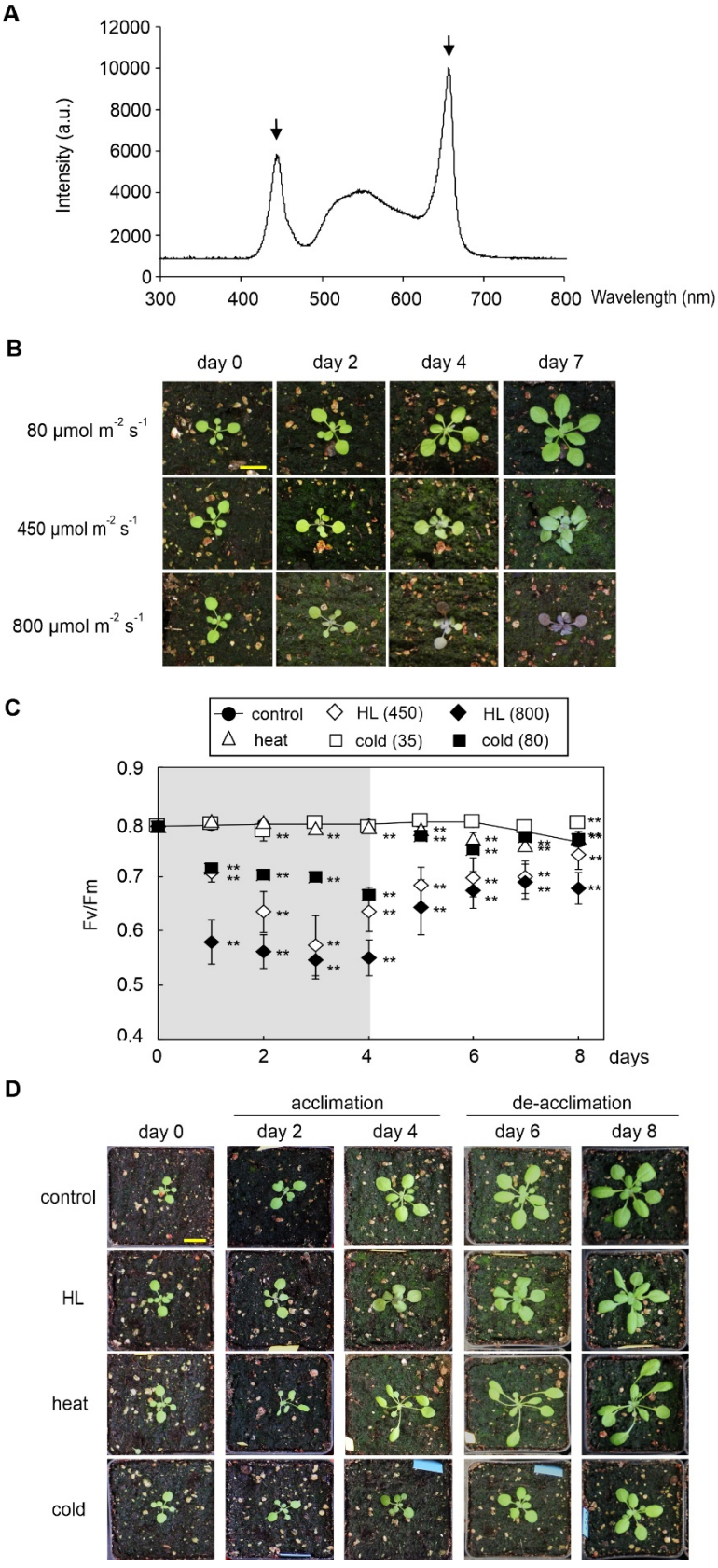

Figure S1. Set-up used to assay for (de-)acclimation to high light, heat and cold conditions, Related to Figure 1.

(A) Spectrum of the LED light source used for Arabidopsis growth. Arrows indicate blue (left) and red (right) peaks.

(B) Growth of Arabidopsis under three different light regimes. Plants were grown for 14 days under standard conditions and exposed to 80, 450 or 800 µmol photons m^{-1} s^{-2} for a further 7 days. Bar = 1 cm.

(**C**) Extent of photoinhibition during acclimation and de-acclimation. Maximum quantum yield of PSII (Fv/Fm) was recorded from plants exposed to standard conditions (control), high light (HL) at 450 or 800 µmol photons m^{-1} s^{-2} (450, 800), heat and cold at 35 or 80 µmol photons m^{-1} s^{-2} (35, 80). Values correspond to the mean ± SD of n ≥ 4 independent experiments. $^{**}P < 0.01$; $^{*}P < 0.05$. See Table S1 for standard deviations and statistics.

(D) Growth of Arabidopsis during exposure (acclimation) to high light (HL), heat and cold, followed by return to control conditions (de-acclimation). Representative plants are shown after 2 and 4 days of acclimation, and a further 2 (day 6) and 4 days (day 8) of de-acclimation. Bar = 1 cm.

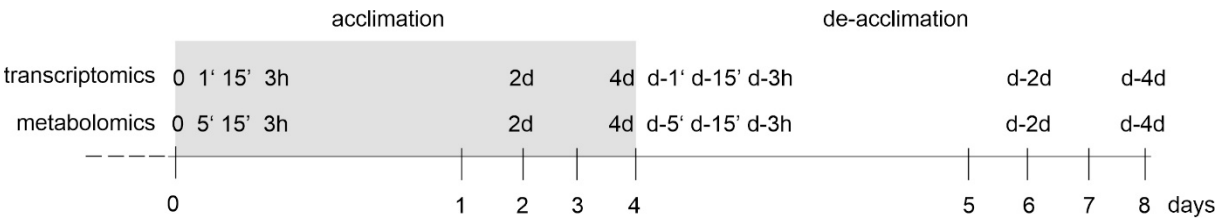

Figure S2. Time-points at which metabolites and transcripts were analyzed, Related to Figures 1, 2 and 3.

Equivalent time-points in the acclimation and de-acclimation phases were selected, and the latter are indicated by the prefix “d-“.

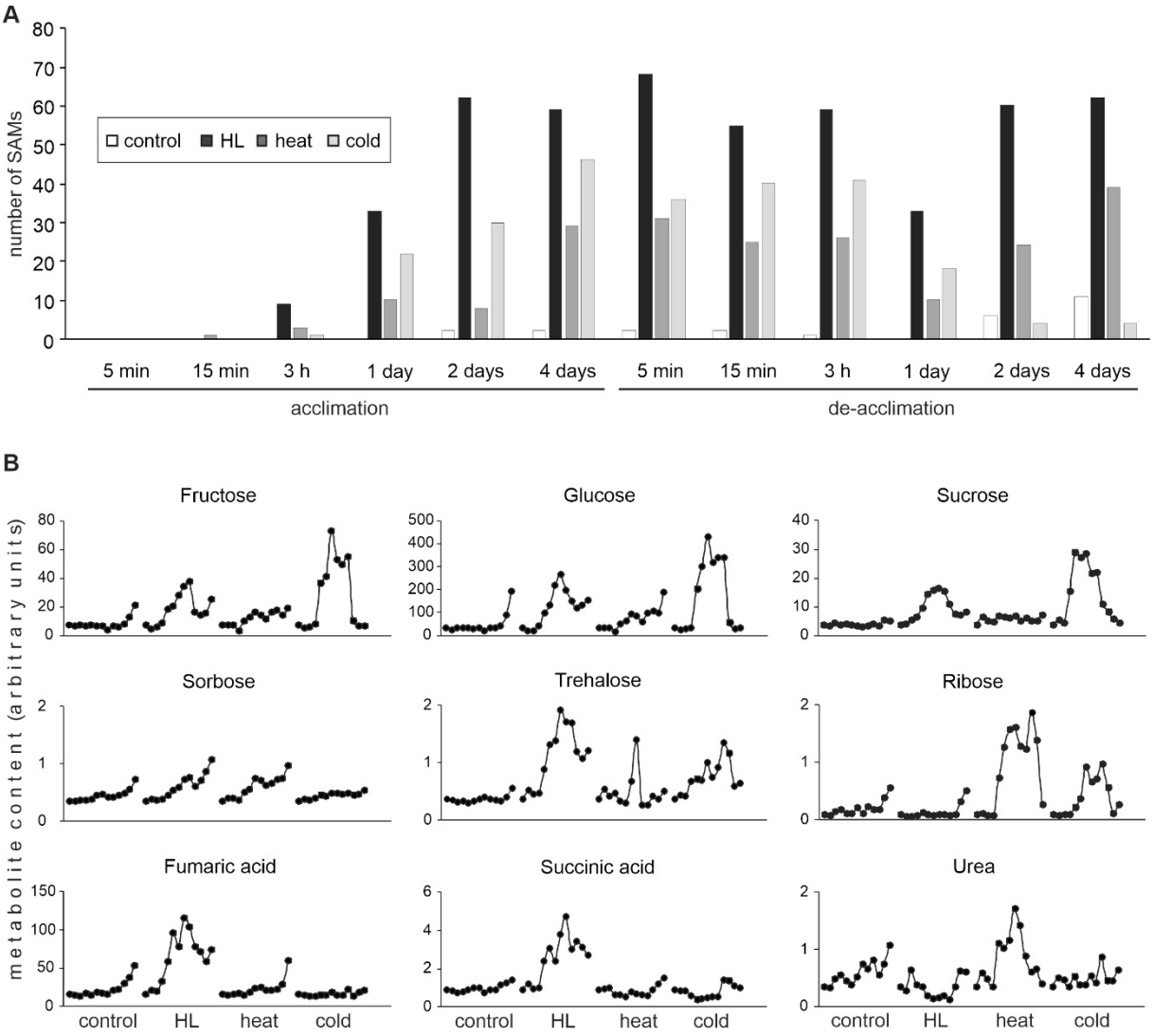

Figure S3. Metabolite changes during acclimation and de-acclimation to high light (HL), heat and cold, Related to Figure 2.

(A) Numbers of significantly altered metabolites (SAMs). SAMs are defined as metabolites that showed at least a twofold change in concentration relative to the initial value at 0 min according to the Student's *t*-test (FDR ≤ 0.05).

(B) Contents of representative metabolites (relative to a ^{13}C sorbitol standard) throughout the time-course under the four conditions. Note that differences between control conditions and treatments are not attributable to changes in periodicity caused by the circadian clock.

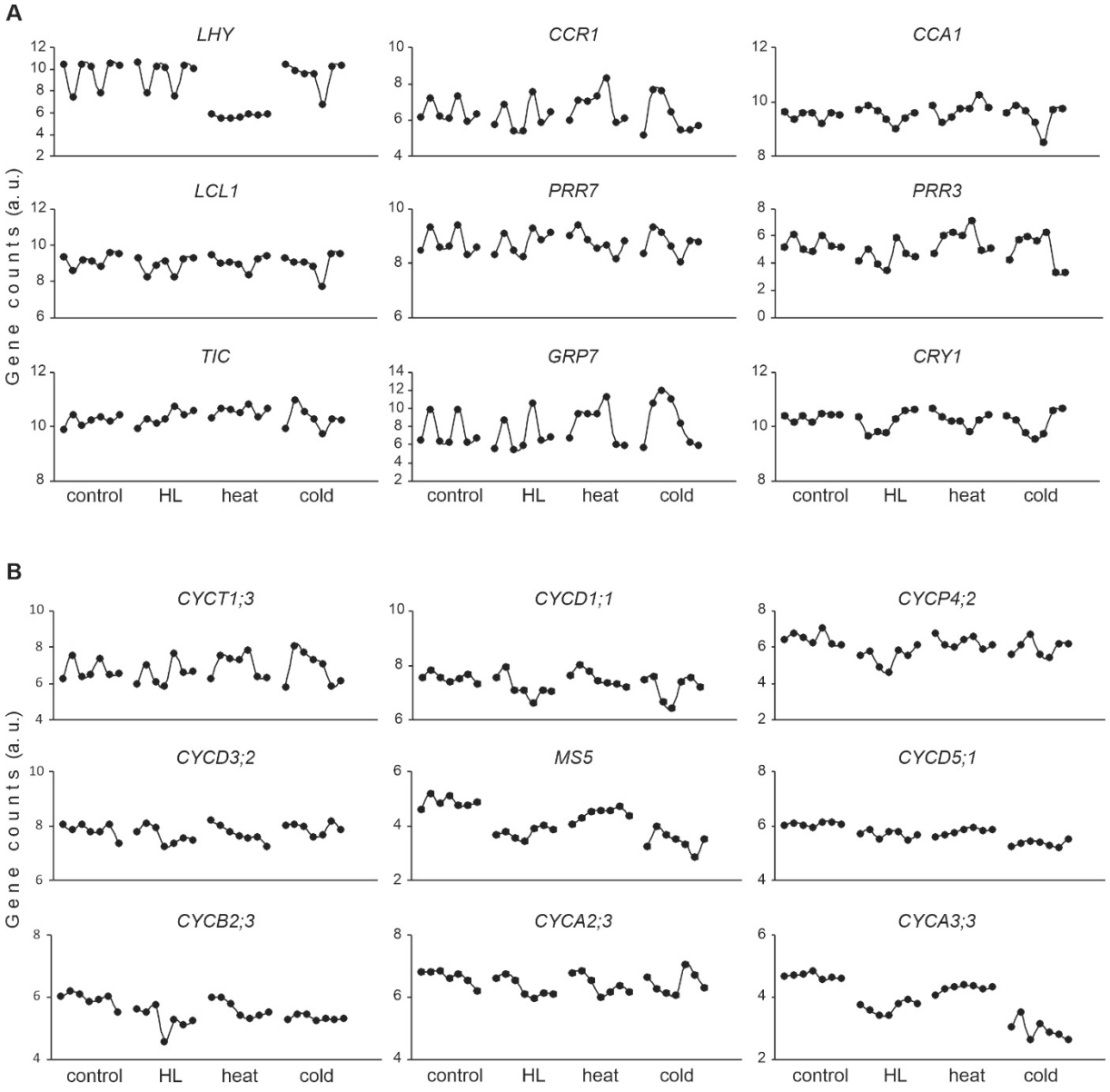

Figure S4. Levels of marker-gene transcripts plotted against circadian-clock time or cell-cycle stage, Related to Figure 3.

(**A**, **B**) The means of normalized counts were used to plot the mRNA expression pattern of *bona-fide* markers for circadian periodicity (**A**) and cell-cycle phase (**B**) at the initial time-point (0 min) and after 3 h, 2 days and 4 days of acclimation and de-acclimation.

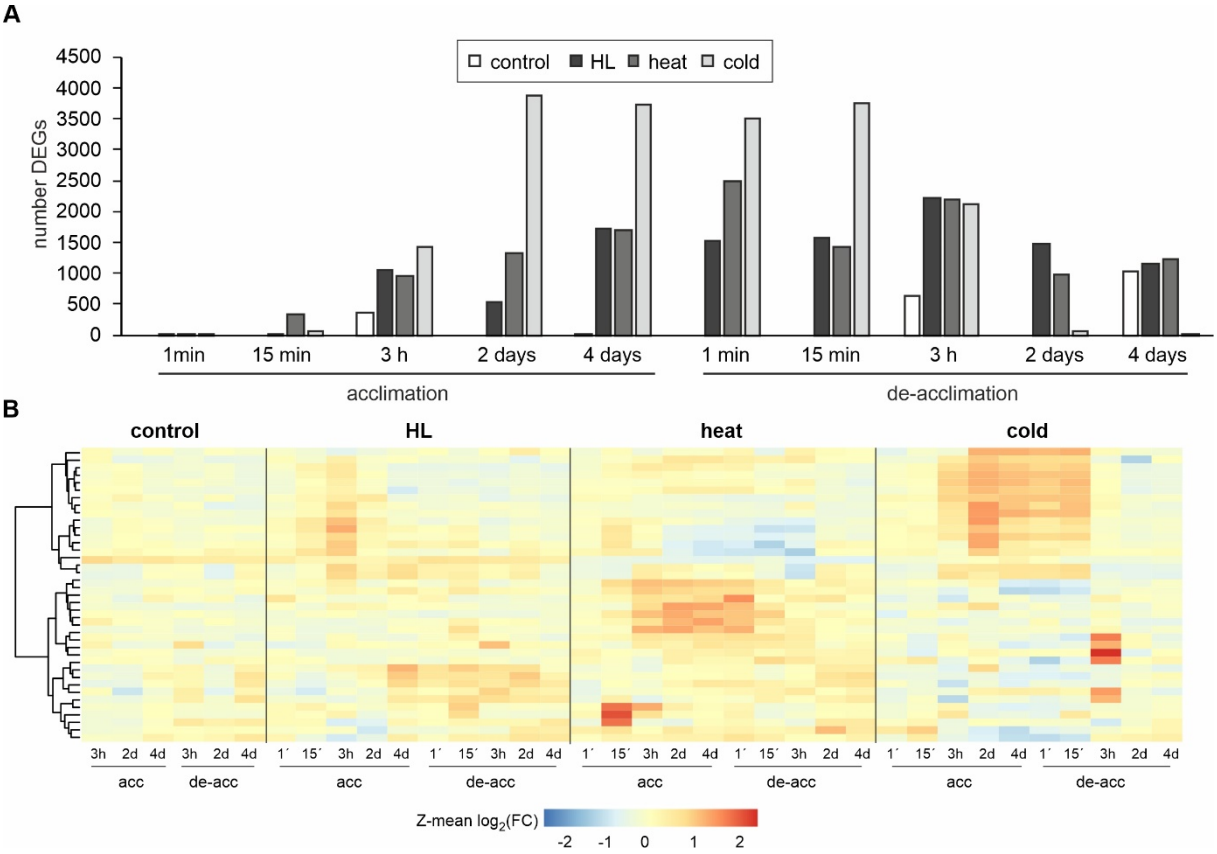

Figure S5. Changes in transcript levels during (de-)acclimation, Related to Figure 3.

(**A**) Differentially expressed genes (DEGs, showing fold changes (FC) ≥ 2 relative to the initial time-point t = 0 (with a false discovery rate [FDR] ≤ 0.05) during control conditions and phases of acclimation and de-acclimation to high light (HL), heat and cold.

(**B**) Heatmap constructed by hierarchical clustering according to the Ward D2 method for DEGs coding for heat-shock proteins and heat-shock factors. Z-means for log_2-converted FC scores under standard conditions, and exposure to HL, heat and cold during acclimation (acc) and de-acclimation (de-acc) phases, were used.

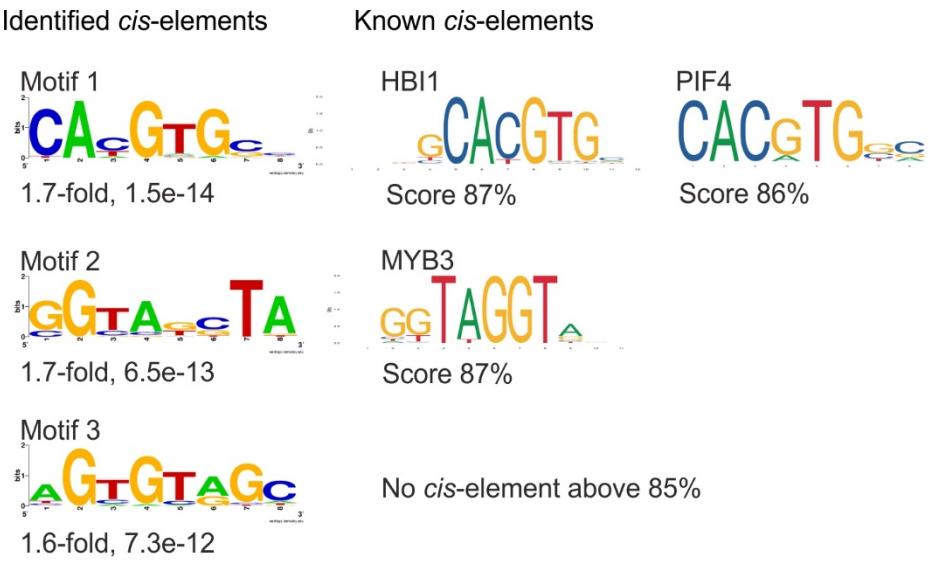

Figure S6. Sequence logos of the most significantly identified *cis*-elements of genes whose expression was regulated under all investigated conditions, Related to Figure 3.

The names of the putative transcription factors binding to the identified *cis*-elements, together with their respective logos, are also shown. Note that motifs can be read in opposite or same direction.

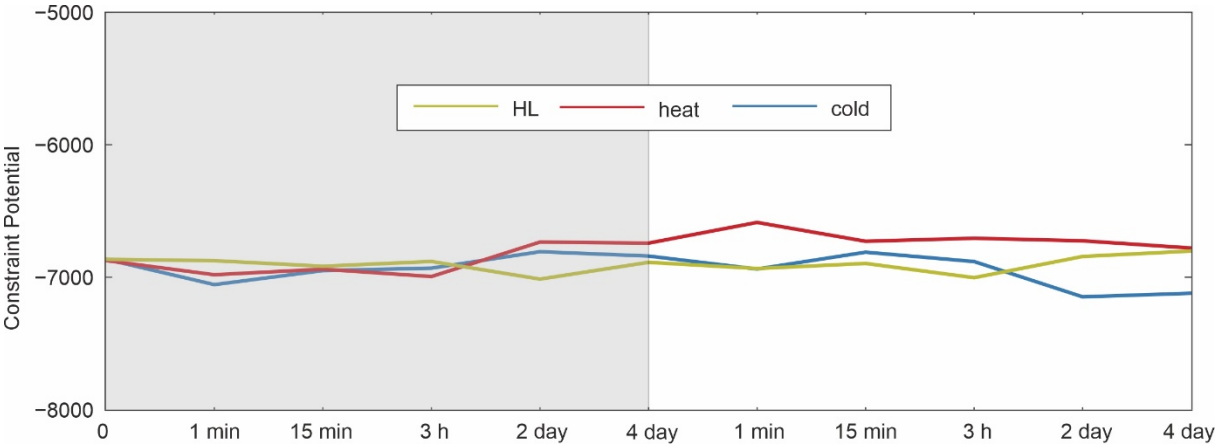

Figure S7. Baseline state for transcriptome changes during (de-)acclimation derived from surprisal analysis, Related to Figure 4.

Time course of the baseline state as determined by surprisal analysis of the transcriptome profiles measured during exposure to high light (HL), heat, or cold treatment and recovery. The acclimation phase is indicated by the gray shading.

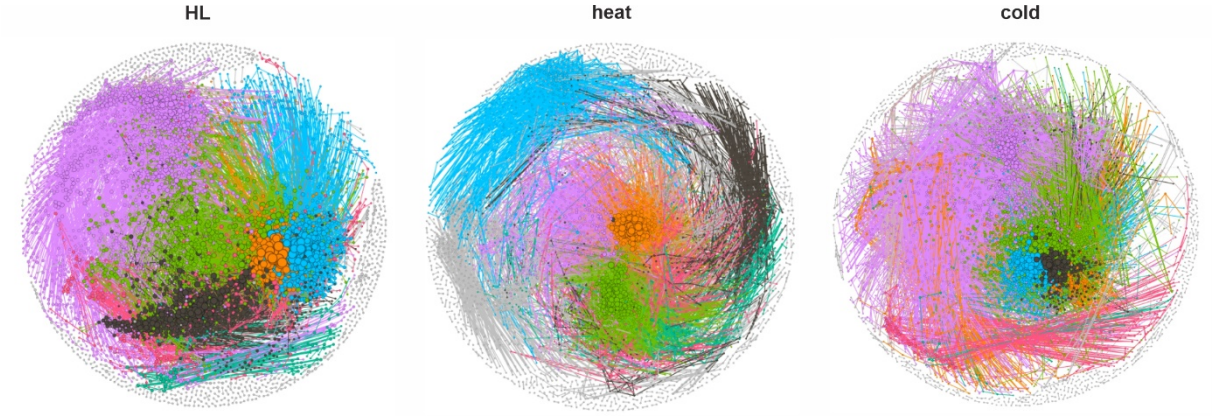

Figure S8. Conditional networks underlying transcriptome changes during (de-)acclimation, Related to Figure 5.

Co-expression of transcriptome changes during acclimation and de-acclimation was assessed by Pearson correlation (R) and mapped onto a reference network. The resulting networks encompass nodes corresponding to transcripts connected by edges ($R \geq 0.9$) as defined in **Experimental Procedures**. The node size is proportional to its degree. Colors indicate network communities. The topological properties of the conditional networks are summarized in **Table S3**.

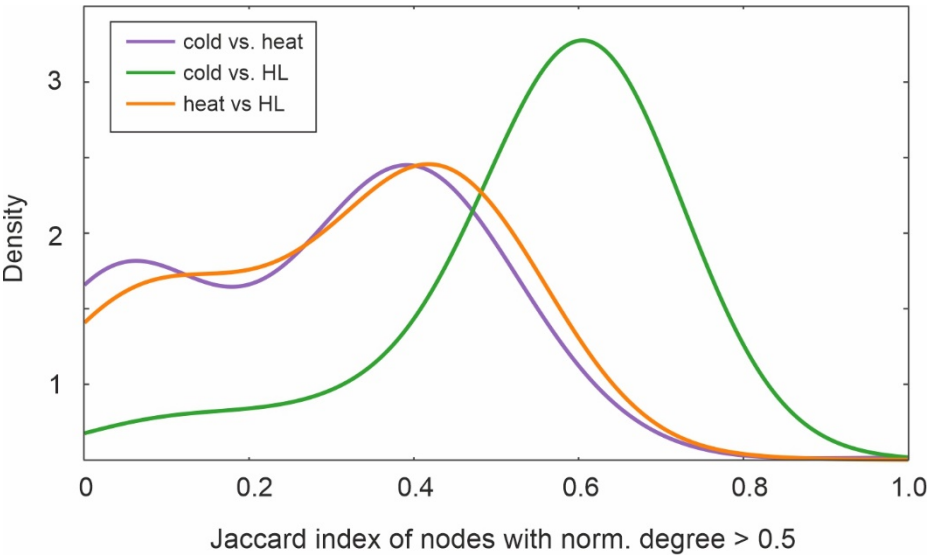

Figure S9. Additional comparison of network topology for transcriptome changes, Related to Figure 5.

Density plot of Jaccard index ($J(A,B)=(|A\cap B|)/(|A|+|B|-|A\cap B|)$, where A is the neighborhood of a node in network A, and B the neighborhood of the same node in network B calculated for the neighborhoods of all nodes in the conditional networks with a normalized degree > 0.5.

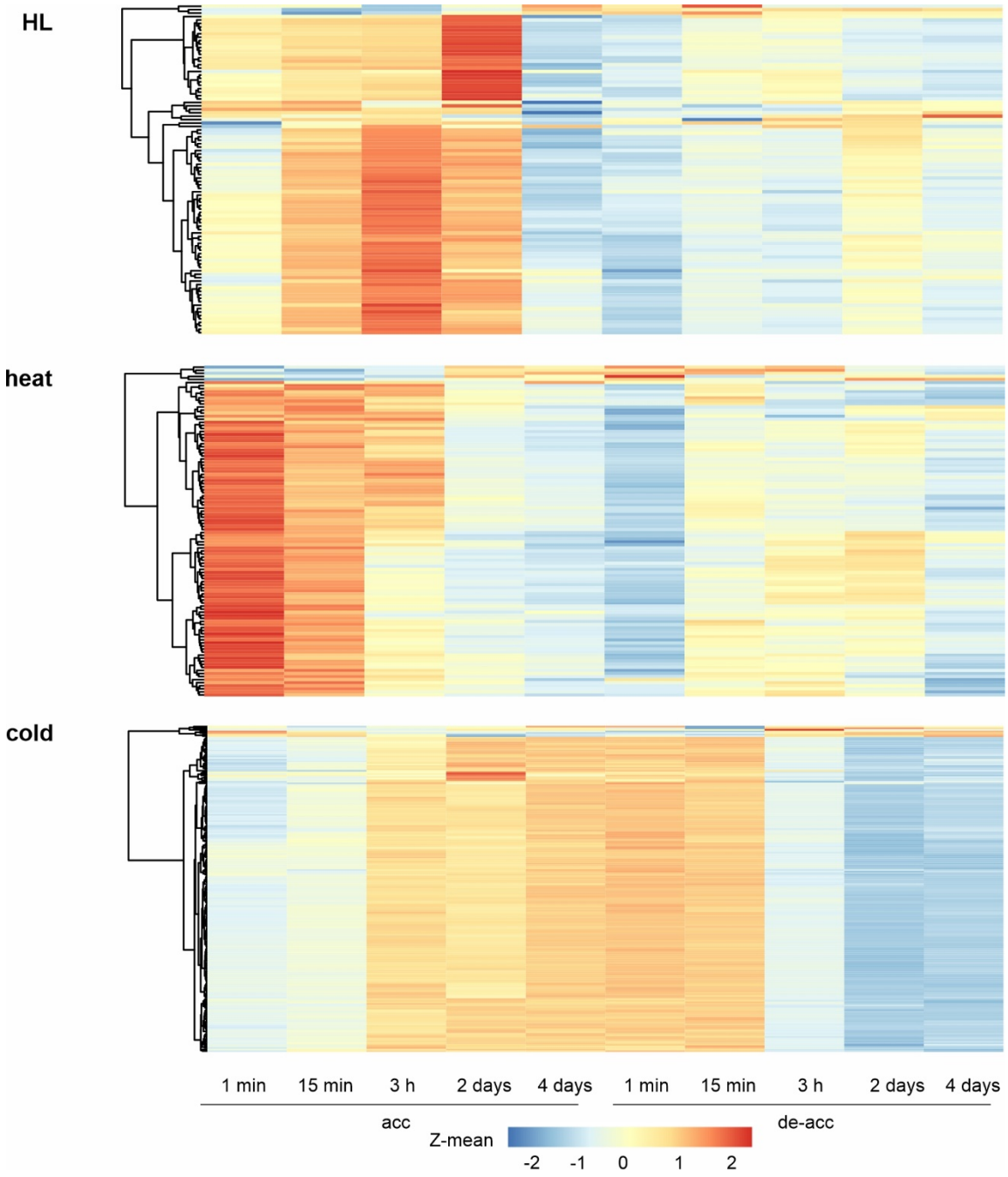

Figure S10. Expression patterns of transcripts for ribosomal proteins (RPs) identified as super-hubs in conditional networks, Related to Figure 6.

Heatmaps obtained by hierarchical clustering according to the Ward D2 method for the RP super-hubs listed in **Table 1**. Z-means were calculated from $\log_2$-transformed fold changes compared to the initial time-point (0 min). acc, acclimation; de-acc, de-acclimation; HL, high light.

Supplemental Tables (Tables S1 to S6, and S9 to S10 are provided as separate Excel files)

Table S7. Overview of DEGs encoding chloroplast proteins, Related to Figure 3. DEGs that behaved similarly in response to high light, heat and cold (de-)acclimation during the central part of the experimental time-courses (from 2 d acclimation to 15 min de-acclimation) and are related to chloroplast functions were sorted according to their molecular roles.

Gene ID	Symbol	Annotation
		Photosynthesis
AT1G29910	Lhcb1.2	Light harvesting chlorophyll a/b binding protein 1.2
AT2G34430	Lhcb1.4	Light-harvesting chlorophyll a/b binding protein 1.4
AT3G27690	Lhcb2.3	Light-harvesting chlorophyll a/b binding protein 2.3
AT5G54270	Lhcb3	Light-harvesting chlorophyll a/b protein 3
AT4G10340	Lhcb5	Light-harvesting complex of photosystem II subunit 5
AT1G15820	Lhcb6	Light-harvesting complex photosystem II subunit 6
AT4G09650	AtpD	F-type H -transporting ATPase subunit delta
AT1G03600	Psb27	Photosystem II family protein
AT3G50820	PsbO2	Photosystem II subunit O2
AT4G21280	PsbQ1	Photosystem II subunit Q1
		Redox
AT1G76100	PETE1	Plastocyanin isoform 1
AT1G20340	PETE2	Plastocyanin isoform 2
AT4G09010	TL29	Ascorbate peroxidase 4
AT1G77490	tAPX	Thylakoidal ascorbate peroxidase
AT3G09580	-	FAD/NAD(P)-binding oxidoreductase family protein
AT1G77510	PDIL1-2	PDI-like 1-2
		Chromophor
AT1G44446	CH1	Pheophorbide a oxygenase family protein
AT1G58290	HEMA1	Glutamyl-tRNA reductase family protein
AT3G14930	HEME1	Uroporphyrinogen decarboxylase
AT4G25080	CHLM	Magnesium-protoporphyrin IX methyltransferase
		Metabolism
AT5G35790	G6PD1	Glucose-6-phosphate dehydrogenase 1
AT1G12900	GAPA-2	Glyceraldehyde 3-phosphate dehydrogenase A subunit 2
AT1G61800	GPT2	Glucose-6-phosphate/phosphate translocator 2
		Others
AT5G57560	TCH4	Xyloglucan endotransglucosylase/hydrolase
AT2G47450	CAO	Chloroplast signal recognition particle component
AT1G31690	-	Copper amine oxidase family protein
AT2G29090	CYP707A2	Cytochrome P450
AT3G09200	-	Ribosomal protein L10 family protein
AT3G50480	HR4	Homolog of RPW8 4
AT1G74710	EDS16	ADC synthase superfamily protein
AT5G01600	FER1	Ferretin 1

Table S8. Topological properties of conditional networks for transcripts, Related to Figure 5. Structural properties of each conditional network, including the numbers of nodes, connections (edges), average degree, modularity and super-hubs (all nodes with more than 100 edges). Note that, due to network complexity, hubs behave as highly interconnected nodes, i.e. *party hubs* (Han et al., 2004) and therefore the product "number hubs x 100" can be higher than the total number of nodes in some networks.

	HL	Heat	Cold
Nodes	5,082	4,634	5,648
Edges	61,800	35,706	110,446
Average degree	16.89	15.41	39.11
Modularity	0.48	0.60	0.40
Super-hubs	371	223	657

Transparent Methods

Plant cultivation and sampling

Arabidopsis thaliana Col-0 seeds were stratified at 4ºC for 2 days, sown in 9x9-cm pots at a density of approximately 50 seeds per pot and cultivated in LED-41 HIL2 cabinets (Percival Scientific, Perry, Iowa, USA) under standard long-day conditions ("control conditions") [LD; 16 h light (80 µmol photons m^{-2} s^{-1}) using 18% white and red LED light intensities (see **Figure S1A** for spectrum) at 22ºC and 8 h darkness at 18ºC]. After 14 days the light intensity was increased to 450 µmol photons m^{-2} s^{-1} (corresponding to 80 % of the white and red LED light intensities) to investigate acclimation to high light (HL). For heat treatment, plants were grown at a constant temperature of 32ºC. In the case of cold treatment, temperature and light intensity were reduced to 4ºC and 35 µmol photons m^{-2} s^{-1}, respectively. In all cases, light was supplied for 18 h per day. Acclimation treatments were started 4 h after light onset and applied for 4 days. Finally, plants were exposed to control conditions for 4 additional days for de-acclimation. Sampling was carried out at the selected time-points (see **Figure S2**) by harvesting of entire shoots following immersion of plantlets in liquid nitrogen. Samples were then ground and stored at -80ºC prior to characterization.

Measurements of physiological parameters

Fresh weight was determined as the mean of groups of 10 plants. Anthocyanin and chlorophyll content was determined as described previously (Mita et al., 1997; Parsons and Strickland, 1963). Chlorophyll *a* fluorescence measurements were conducted using the IMAGING-PAM M-Series instrument (Walz, Effeltrich, Germany) on plants that had been dark-adapted for 30 min. After determining the minimal fluorescence (F_o), a saturation pulse of actinic light (0.5 s; 2700 µmol photons m^{-2} s^{-1}; 450 nm) was applied to determine the maximum fluorescence (F_m) and the maximum quantum yield of photosystem II (PSII) (F_v/F_m; calculated as $(F_m - F_o)/F_m$).

The effective quantum yield of PSII ($\Phi_{II} = (F_m' - F_0')/F_m']$) and non-photochemical quenching (NPQ; calculated as (Fm-Fm')/Fm')) were monitored at 80 μmol photons m^{-2} s^{-1} every 2 sec for 5 min (Armbruster et al., 2010) and the value at 260 s is depicted in the Figures.

RNA isolation, transcriptome profiling and data analysis

Total RNA from aerial parts of plants was isolated using *Trizol* (Invitrogen, Carlsbad, Calif., USA) using 1 part plant to 15 parts reagent (w/v), and purified on *Direct-zol™ RNA MiniPrep Plus* columns (Zymo Research, Irvine, Calif., USA) according to the manufacturer's instructions. RNA integrity and quality were assessed by gel electrophoresis using the Agilent 2100 Bioanalyzer (Agilent, Santa Clara, Calif., USA). Only those samples with an RNA Integrity Number (RIN) ≥ 7 were further processed. Ribosomal RNA depletion, generation of RNA-Seq libraries and 150-bp sequencing of long-non-coding (lnc) RNAs using the paired-end mode were conducted by *Novogene Biotech* (Beijing, China) with standard Illumina protocols. The RNA-Seq libraries were sequenced on an Illumina HiSeq 2500 system (Illumina, San Diego, Calif. USA). Three independent biological replicates were used per time-point and treatment.

RNA-Seq datasets were analyzed as follows: adaptor removal and sequencing quality was carried out with *Trimmomatic* (Bolger et al., 2014) and *FastQC* (http://www.bioinformatics.babraham.ac.uk/projects/fastqc/), respectively. Reads were mapped to the Arabidopsis genome (TAIR10) with *Tophat 2.1.1* (Kim et al., 2013) for First Read (FR) unstranded libraries, adjusting the maximum intron length to 3000 bp. Reads were counted with *featureCounts* (Liao et al., 2014) according to the gene annotation in Araport11 (www.araport.org/data/araport11). Differentially expressed genes (DEGs) were obtained with *DESeq2* (Love et al., 2014) by comparing each time-point of the treatments with the initial time point (0 min).

All transcriptome datasets were deposited at the Gene Expression Omnibus (GEO; https://www.ncbi.nlm.nih.gov/geo/) under the accession number GSE125950.

Metabolite isolation, metabolome profiling and data analysis

Polar primary metabolites were identified in 14-day-old plants and at the indicated times after transfer to acclimation and de-acclimation conditions. To this end, metabolites were extracted from 50-mg samples of frozen rosettes (n = 6 plants from 6 independent experiments) and derivatized as described previously (Erban et al., 2007; Lisec et al., 2006; Rossel et al., 2002). Ribitol (0.2 mg mL^{-1} in water) and ^{13}C-labeled sorbitol (0.2 mg mL^{-1} in water) served as internal standards for relative quantification. The derivatized samples were injected into a gas chromatograph coupled to a time-of-flight mass spectrometer (GC-TOF-MS) system (Pegasus HT, Leco, St Joseph, Mich., USA) and chromatographic separation was performed on an Agilent GC 7890A, using a 30 m VF-5ms column with 10 m EZ-Guard column. Mass spectra were recorded at 20 scans s^{-1} with an 50-800 m/z scan range and evaluated using ChromaTOF 4.5 and TagFinder 4.1 (Luedemann et al., 2008) and the compounds were manually annotated based on the Golm Metabolome Database (Kopka et al., 2005).

Surprisal analysis

Surprisal analysis is a thermodynamic approach that yields a biophysicochemical understanding and quantitative characterization of biological systems using a molecule-centered approach. The key step in surprisal analysis is the definition of a balanced state, i.e., the steady-state of the system that has the maximum entropy. Surprisal analysis then allows one to identify deviations of molecule levels with respect to the balanced state, which are quantified by constraints that characterize their responses. The surprisal $I(x)$ of each individual transcript $x_1 \ldots x_i$ at the time-point t is defined as the deviation from the individual transcript's

contribution to the baseline state x_i^0: $I(x) = -\ln(\frac{x_i(t)}{x_i^0})$. This is achieved by fitting the surprisal using a number of terms, $-\sum_{\alpha=1} G_{i\alpha}\,\lambda_\alpha(t)$, where α is the index of the constraint, $G_{i\alpha}$ is the weight of the transcript x_i in constraint G_α, and $\lambda_\alpha(t)$ is the Lagrange multiplier for G_α that is being varied to find the best fit. This is achieved as described by Remacle et al. (2010) using the singular value decomposition. Raw count data from the transcriptome datasets for each experimental condition were averaged across replicates. To deal with counts equal to 0, all counts were increased by 1. Subsequently, the resulting count means were normalized using the FPKM (Fragment Per Kilobase Million) method. Surprisal analysis was performed as described by Remacle et al. (2010) on the preprocessed datasets transformed into the natural logarithm space using the F# implementation available in the *FSharp.Stats* package (https://github.com/CSBiology/FSharp.Stats @ v0.1.1).

For constraint-based time-course comparisons between experimental conditions, linear regression of each constraint potential was calculated against all conditions using the *FSharp.Stats* package. The coefficient of determination (R^2) of these regressions was then weighted using the mean of the respective constraint weights (the singular values obtained by surprisal analysis).

Construction of conditional networks

Correlation Networks of the respective conditions were elaborated from the transcription profiles. To this end, pairwise Pearson correlations (R) among the mean FPKM values for each transcript were computed, and the subsequent correlation matrix was used to construct the network. Subsequently, Random Matrix Theory (RMT) (Luo et al., 2007) implemented in the *FSharp.Stats* package was used to find an optimal threshold to filter out spurious correlations and noise. Accordingly, absolute values of R = 0.9003, 0.9106 and 0.9116 were used for the data from HL, heat and cold treatments, respectively. To further constrain the correlation

network, the topological overlap of the filtered correlation networks with the structural and functional reference network ARANet v2 (Lee et al., 2015) (https://www.inetbio.org/aranet/downloadnetwork.php) was computed by filtering edges that were not present in the reference network. The resulting networks contain specific information about the experimental condition and general information about structure- function relations in *Arabidopsis thaliana* and are therefore termed conditional networks. Networks were visualized and analyzed in Gephi (https://gephi.org/).

To assess conditional network similarity between experimental conditions, all node degrees were normalized to the highest degree and filtered for overlapping nodes for each comparison. Pearson correlations of normalized node degrees of these overlapping nodes were calculated using the *FSharp.Stats* package.

Further bioinformatic analyses

Partial Least Squares (PLS) regression analysis was performed using the *plsdepot* R package (https://CRAN.R-project.org/package=plsdepot @ v0.1.17), extracting the first two components without crossvalidation, and using the constraint potentials obtained by surprisal analysis as predictors for the physiological parameters of the respective condition (responses).

Differences in transcripts were estimated according to DESeq2, as mentioned above. Metabolome datasets were filtered by one-way ANOVA (FDR ≤ 0.05) to exclude differences due to sample variability, and Student´s t-test was applied. In all cases, pairwise comparisons of each time-point for the treatments against the respective control were considered. Significant differences in transcripts (DEGs) and metabolites (SAMs) were defined by applying a cut-off of an absolute $\log_2$-fold change (FC) ≥ 1 and a false discovery rate (FDR) of ≤ 0.05 after applying the multiple testing Benjamini-Hochberg procedure (Benjamini and Hochberg, 1995). Heat maps with hierarchical clustering according to the Ward D2 method were elaborated using Z-mean values using the *pheatmap* package integrated in RStudio

(https://www.bioconductor.org). Venn diagrams were elaborated in the interface Venny 2.1 (Oliveros, 2007-2015) and the significance of overlaps was calculated with the RStudio package *SuperExactTest* (Wang et al., 2015). Gene Ontology (GO) enrichments were obtained from the *Database for Annotation, Visualization and Integrated Discovery* (DAVID) (Huang da et al., 2009a, b), applying a cut-off of 2-fold enrichment compared to the expected frequency in the Arabidopsis genome and an FDR (Benjamini-Hochberg) of ≤ 0.05. Non-redundant GO terms were selected in the interface REVIGO using the small similarity (0.5) parameter (Supek et al., 2011). Significance of enrichments were calculated with Fisher's exact test with the *stat* and package (RStudio).

Supplemental References

Armbruster, U., Zühlke, J., Rengstl, B., Kreller, R., Makarenko, E., Rühle, T., Schünemann, D., Jahns, P., Weisshaar, B., Nickelsen, J., *et al.* (2010). The Arabidopsis thylakoid protein PAM68 is required for efficient D1 biogenesis and photosystem II assembly. Plant Cell *22*, 3439-3460.

Benjamini, Y., and Hochberg, Y. (1995). Controlling the false discovery rate: a practical and powerful approach to multiple testing. J R Statist Soc B *57*, 289-300.

Bolger, A.M., Lohse, M., and Usadel, B. (2014). Trimmomatic: a flexible trimmer for Illumina sequence data. Bioinformatics *30*, 2114-2120.

Erban, A., Schauer, N., Fernie, A.R., and Kopka, J. (2007). Nonsupervised construction and application of mass spectral and retention time index libraries from time-of-flight gas chromatography-mass spectrometry metabolite profiles. Methods Mol Biol *358*, 19-38.

Han, J.D., Bertin, N., Hao, T., Goldberg, D.S., Berriz, G.F., Zhang, L.V., Dupuy, D., Walhout, A.J., Cusick, M.E., Roth, F.P., *et al.* (2004). Evidence for dynamically organized modularity in the yeast protein-protein interaction network. Nature *430*, 88-93.

Huang da, W., Sherman, B.T., and Lempicki, R.A. (2009a). Bioinformatics enrichment tools: paths toward the comprehensive functional analysis of large gene lists. Nucleic Acids Res *37*, 1-13.

Huang da, W., Sherman, B.T., and Lempicki, R.A. (2009b). Systematic and integrative analysis of large gene lists using DAVID bioinformatics resources. Nat Protoc *4*, 44-57.

Kim, D., Pertea, G., Trapnell, C., Pimentel, H., Kelley, R., and Salzberg, S.L. (2013). TopHat2: accurate alignment of transcriptomes in the presence of insertions, deletions and gene fusions. Genome Biol *14*, R36.

Kopka, J., Schauer, N., Krueger, S., Birkemeyer, C., Usadel, B., Bergmuller, E., Dormann, P., Weckwerth, W., Gibon, Y., Stitt, M., *et al.* (2005). GMD@CSB.DB: the Golm Metabolome Database. Bioinformatics *21*, 1635-1638.

Lee, T., Yang, S., Kim, E., Ko, Y., Hwang, S., Shin, J., Shim, J.E., Shim, H., Kim, H., Kim, C., *et al.* (2015). AraNet v2: an improved database of co-functional gene networks for the study of *Arabidopsis thaliana* and 27 other nonmodel plant species. Nucleic Acids Res *43*, D996-1002.

Liao, Y., Smyth, G.K., and Shi, W. (2014). featureCounts: an efficient general purpose program for assigning sequence reads to genomic features. Bioinformatics *30*, 923-930.

Lisec, J., Schauer, N., Kopka, J., Willmitzer, L., and Fernie, A.R. (2006). Gas chromatography mass spectrometry-based metabolite profiling in plants. Nat Protoc *1*, 387-396.

Love, M.I., Huber, W., and Anders, S. (2014). Moderated estimation of fold change and dispersion for RNA-seq data with DESeq2. Genome Biol *15*, 550.

Luedemann, A., Strassburg, K., Erban, A., and Kopka, J. (2008). TagFinder for the quantitative analysis of gas chromatography--mass spectrometry (GC-MS)-based metabolite profiling experiments. Bioinformatics *24*, 732-737.

Luo, F., Yang, Y., Zhong, J., Gao, H., Khan, L., Thompson, D.K., and Zhou, J. (2007). Constructing gene co-expression networks and predicting functions of unknown genes by random matrix theory. BMC Bioinformatics *8*, 299.

Mita, S., Murano, N., Akaike, M., and Nakamura, K. (1997). Mutants of *Arabidopsis thaliana* with pleiotropic effects on the expression of the gene for beta-amylase and on the accumulation of anthocyanin that are inducible by sugars. Plant J *11*, 841-851.

Oliveros, J.C. (2007-2015). Venny. An interactive tool for comparing lists with Venn's diagrams. (https://bioinfogp.cnb.csic.es/tools/venny/index.html).

Parsons, T.R., and Strickland, J.D.H. (1963). Discussion of spectrophotometric determination of marine-plant pigments, with revised equations for ascertaining chlorophyll-a and carotenoids. J Marine Res *21*, 105-156.

Remacle, F., Kravchenko-Balasha, N., Levitzki, A., and Levine, R.D. (2010). Information-theoretic analysis of phenotype changes in early stages of carcinogenesis. Proc Natl Acad Sci U S A *107*, 10324.

Rossel, J.B., Wilson, I.W., and Pogson, B.J. (2002). Global changes in gene expression in response to high light in Arabidopsis. Plant Physiol *130*, 1109-1120.

Supek, F., Bosnjak, M., Skunca, N., and Smuc, T. (2011). REVIGO summarizes and visualizes long lists of gene ontology terms. PLoS One *6*, e21800.

Wang, M., Zhao, Y., and Zhang, B. (2015). Efficient test and visualization of multi-set intersections. Sci Rep *5*, 16923.